National University of Science and Technology
POLITEHNICA Bucharest
Faculty of Chemical Engineering and Biotechnologies
Doctoral School Chemical Engineering and Biotechnologies

Ph.D. Thesis
- Summary -

Photo-oxidative degradation of organic compounds from wastewater

PhD Student:
Eng. Giovanina-Iuliana LUPU (IONICĂ)

Research Supervisor:
Prof. Dr. Eng. Cristina ORBECI

Bucharest, 2023

CONTENT

INTRODUCTION

In recent years, the presence of organic compounds that are difficult or impossible to biodegrade in wastewater has been a major problem, posing a threat to the environment and public health. Attention has been focused on the degradation/removal of these organic compounds from wastewater due to their toxicity, as well as their negative effects on the environment.

The doctoral thesis entitled "Photo-oxidative degradation of organic compounds from wastewater" is structured in two parts, namely A. Literature review and B. Experimental study - original contributions. In the literature review, advanced oxidation processes were presented synthetically, with emphasis on the most commonly used processes, photocatalysis and Fenton processes, which were also addressed in the experimental part, so that their use made it possible to evaluate the photocatalytic activity of the functionalized materials synthesized as part of the experimental research carried out within this doctoral thesis.

In the first chapter are presented the main advanced oxidation processes and their applications, as well as the limitations and factors that influence the optimal development of these processes, are presented. In the continuation of this chapter, the most common methods for obtaining functionalized materials are presented, the chapter ending with a series of partial conclusions.

Chapter 2 presents the two classes of target organic compounds chosen in the studies of photocatalytic oxidation carried out in this doctoral thesis. This chapter is ending with the main partial conclusions drawn from the structure of the study.

Chapter 3 highlights the main purpose of the PhD thesis and the specific objectives derived from it. Each specific objective is then covered in a separate chapter in the thesis.

Chapter 4 represents the first specific objective, namely the synthesis and characterization of TiO_2/stainless steel functionalized materials used in the study of photocatalytic oxidation of phenolic organic compounds from wastewater. The chapter is ending with a series of partial conclusions resulting from the experimental research carried out for the elaboration of this chapter.

Chapter 5 is represented by the second specific objective, namely the obtaining and characterization of two functionalized materials type TiO_2/Ti and Co-doped TiO_2/polymer and their evaluation in the study of photocatalytic oxidation of phenolic organic compounds from wastewater. The chapter is ending with the partial conclusions resulting from the experimental study conducted.

Chapter 6 is represented by the third specific objective, namely the synthesis and characterization of a series of TiO_2/fiberglass functionalized materials and the evaluation of each functionalized material obtained in the studies of photocatalytic degradation of pharmaceutical organic compounds from wastewater. The chapter is ending with a series of partial conclusions drawn after the completion of the experimental study conducted in this chapter.

Chapter 7 is represented by the fourth specific objective, namely the obtaining and characterization of TiO_2/fiberglass type stratified network and Nb-doped TiO_2/fiberglass type stratified network functionalized materials and the evaluation of these functionalized materials obtained in the study of the photocatalytic degradation of azithromycin from wastewater. In the ending, this chapter presents the partial conclusions drawn after the realization of the experimental study conducted for the elaboration of this chapter.

Chapter 8 is represented by the fifth specific objective, namely the obtaining and characterization of new TiO_2/fiberglass type mesh and Nb-doped TiO_2/fiberglass type mesh functionalized materials Nb and $FeCl_3$ doped TiO_2/fiberglass type mesh and the evaluation of the photocatalytic activity of the new obtained materials in the study of the photocatalytic oxidation of azithromycin. The chapter is ending with the main conclusions drawn from the experimental study of this chapter.

Chapter 9 is represented by the last specific objective, namely the obtaining and characterization of functionalized nanocomposite materials based on cellulose acetate combined with graphene oxide and PTFE coating with TiO_2 covered. The obtained materials

were tested in the study of the photocatalytic oxidation of azithromycin. In the ending, this chapter presents the partial conclusions drawn after the performance of this experimental study.

The last chapter, namely chapter 10, presents the general conclusions drawn after the elaboration of the doctoral thesis.

The doctoral thesis is ending with the presentation of the original contributions and the exposition of the directions and perspectives for further development, the presentation of the list of published scientific papers and under publication papers, the list of international conferences and activities carried out during the doctoral studies, as well as the list of bibliographic references.

The thesis contains 109 figures, 15 tables and 114 bibliographic references.

The results of this doctoral thesis were exploited through three publications, of which 1 scientific article in the Scientific Bulletin of National University of Science and Technology POLITEHNICA Bucharest and 2 scientific articles in ISI journals. Also, the research results were presented at 6 international conferences, three in the year 2023 and three in the year 2022.

Keywords: functionalized materials, photocatalytic degradation, organic compounds, photocatalysis, photocatalysts deposited on supported material

ORIGINAL CONTRIBUTIONS

Chapter IV – TiO_2/stainless steel functionalized materials for the degradation of phenolic organic compounds from wastewater

IV.1 Specific objective

The objective of this chapter was to study the influence of operating parameters for the photocatalytic degradation of 2,4-dicholorophenol (2,4-DCF) using a TiO_2/stainless steel functionalized material. The specific objectives of this study focused on the following:

- identify the optimal pH of the working solution for the photocatalytic degradation of 2,4-DCF;
- identify the optimal molar ration of H_2O_2/2,4-DCF;
- establishing the initial concentration of the organic compound (2,4-DCF)

IV.2 Materials and methods

In the experimental study, it was used synthetic solutions containing 2,4-dichlorophenol (Fluka Chemicals) as the organic substrate, 30% hydrogen peroxide by volume as the oxidation agent, and 0.1N sulfuric acid for pH adjustment (Sigma-Aldrich).

Chemical oxygen demand (COD) analysis was performed by using potassium dichromate ($K_2Cr_2O_7$), mercuric sulfate ($HgSO_4$), silver sulfate (Ag_2SO_4), potassium acid phthalate ($C_8H_5KO_4$), as well as sulfuric acid 95–97% by mass, all of them of analytical grade purchased from Sigma-Aldrich.

The photocatalytic degradation experiments were carried out in a laboratory installation used for the photocatalytic oxidation of the organic substrate, consisting of a tubular photocatalytic reactor, equipped with a water-cooling jacket, a UV lamp, an external centrifugal pump that ensures the recirculation of the working solution containing the organic compound throughout the irradiation period, a solution storage vessel and a UV lamp power supply.

The UV lamp and photocatalytic membranes were positioned coaxially in the reactor, with the UV lamp being placed inside the photocatalytic membrane (cylindrical shape) having a nominal power of 120 W, which results in the membrane absorbing a radiant energy of 1.5 W/cm.

The working solution containing the organic compound, with a volume of 2.5 L, was continuously recirculated for 2 hours with the help of the centrifugal pump, with an average recirculation flow rate of 1 L/min.

The recirculation pump takes the working solution containing the organic compound from the storage vessel and feeds the reactor at the bottom, thus allowing the membrane to be completely immersed in the working solution. The reactor, with a volume of 1.5 L, is provided with an outer jacket necessary for the countercurrent circulation of the cooling agent, i.e. tap water. Since the working solution is continuously recirculated through the centrifugal pump, it is necessary for its passage through the recirculation vessel to have an additional volume of working solution.

The functionalized material is made from a stainless-steel grid support (cylindrical shape, 10 cm×30 cm) on which TiO_2 (P25 from Degussa, Essen, Germany) was deposited by electrophoretic deposition.

IV.3 Structural and morphological characterization of TiO_2/stainless steel functionalized materials

For the structural and morphological characterization of the functionalized material used in the study of photocatalytic degradation of 2,4-DCF were realized FTIR and SEM-EDX analyses.

In figure 15 is presented the FTIR spectra for the TiO_2/stainless steel functionalized material.

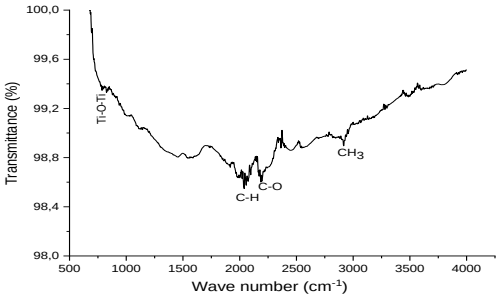

Figure 15. FTIR spectra for TiO_2/stainless steel

FTIR spectra for TiO_2/stainless steel functionalized material indicated the presence of TiO_2 in the structure of the functionalized material. The peak value of about 826 cm^{-1} indicates the presence of Ti-O-Ti bond, and the presence of C-H bond can be attributed a peak value of about 2030 cm^{-1}. The presence of CH_3 group can be attributed to a peak value of approximately 2918 cm^{-1}. The value of about 2185 cm^{-1} can be attributed to the C-O simple bond.

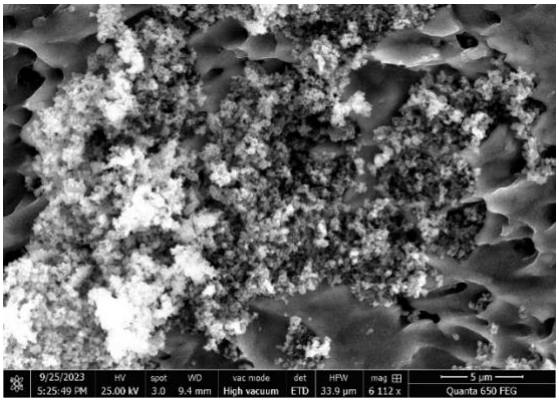

Figure 16. SEM image for TiO_2/stainless steel

For the TiO_2/stainless steel functionalized material, the SEM image (figure 16) indicates an agglomeration of TiO_2 particles in the cavities on the steel surface. Thus, the deposition of particles is uneven on the surface of the material, but the degree of adhesion to the surface is high, which give it a higher stability during the photocatalytic process. This type of deposition is specific to electrophoretic process.

IV.4 Testing of prepared materials in the study of photocatalytic degradation of 2,4-dichlorophenol

- Evaluation of photocatalytic degradation of prepared materials

Photocatalytic degradation was realized by monitoring the evolution of the organic content of the working solution as a function of irradiation time. Thus, samples of about 10 mL were taken from reactor at predetermined irradiation times. After the solutions were prepared, their pH was adjusted to the set value and the amount of hydrogen peroxide (calculated in advance) was added. The results obtained in both the adsorption experiments in the absence of UV light and the results of the photo-oxidative degradation experiments are presented below.

- Kinetic of photo-oxidative degradation

Because the photocatalytic oxidation process mainly involves two stages, one of adsorption of the organic compound on the catalyst surface and another of photocatalytic oxidation itself, the experimental results were interpreted based on the Langmuir– Hinshelwood (L-H) model which considers these two main stages.

The Langmuir-Hinshelwood model was initially used to quantitatively describe solid–gas reactions. Currently the Langmuir-Hinshelwood model is also used to describe the kinetics of reactions that take place in the solid–liquid system by a rate law in which the reaction rate (r) is directly proportional to the fraction of surface area occupied by the substrate (θ):

$$r = -\frac{dC}{dt} = k\theta \quad (10)$$

Considering the form of the Langmuir equation: $\theta = \frac{KC}{1+KC}$ (11) and substituting in the above equation obtains: $r = -\frac{dC}{dt} = k\theta = \frac{kKC}{1+KC}$ (12)

Where: k represents the rate constant, which is influenced by several parameters including catalyst mass, photon flux, etc. K represents the Langmuir–Hinshelwood equilibrium adsorption constant.

Usually, the value of K is obtained from the Langmuir equation from kinetic studies performed in the presence of light, the results being much better than those obtained from studies in the dark. C represents the concentration of the organic substrate at time t. By integration, the above equation becomes:

$$\ln\left(\frac{C_0}{C}\right) + K(C_0 - C) = kKt \quad (13)$$

where C_0 represents the initial concentration of the organic substrate, and t represents the irradiation time $(C_0\text{-}C) = kt$ (14)

$$-\frac{dC}{dt} = k_{ap}\, c \quad (15)$$

The linearized form of the above equation is described by the equation:

$$ln\frac{C_0}{C} = k_{ap}t \quad (16)$$

$$t_{1/2} = \ln\frac{2}{k_{ap}} \quad (17)$$

By graphically representing the term ln (C_0/C) as a function of the irradiation time t, a line is obtained whose slope represents the apparent rate constant, k_{ap}. Its value can be used to calculate the half-life t1/2. By the graphical representation of the term ln (C0-C) as a function of short irradiation times, it is possible to identify the area in which the reaction takes place after a kinetics of pseudo-zero order. By multiplying the apparent rate constant k_{ap} obtained from the slope of the graph ln (C_0/C) as a function of the irradiation time with the initial concentration of organic substrate C_0, the value of the initial reaction rate r_0 is obtained for pseudo-first-order kinetics. This value can be used for comparison with other values of reaction rates obtained under various experimental conditions.

- The influence of pH of the working solution

The initial rate values were calculated according to the methodology described above and were plotted as a function to the initial concentration of 2,4-DCF expressed in terms of organic carbon (Figure 21a) for the four pH values of the working solution. To determine the kinetic parameters, the linearized form of the Langmuir–Hinshelwood model was used (Figure 21b). Figure 21b shows that for all pH values in the chosen concentration range (18.5–112.5 mg OC/L), there is a linear dependence characterized by regression coefficients with values close to unity. Table 7 shows the values of the kinetic parameters obtained for the three pH values of the working solution at a hydrogen peroxide/chlorophenol molar ratio (N) of 1.

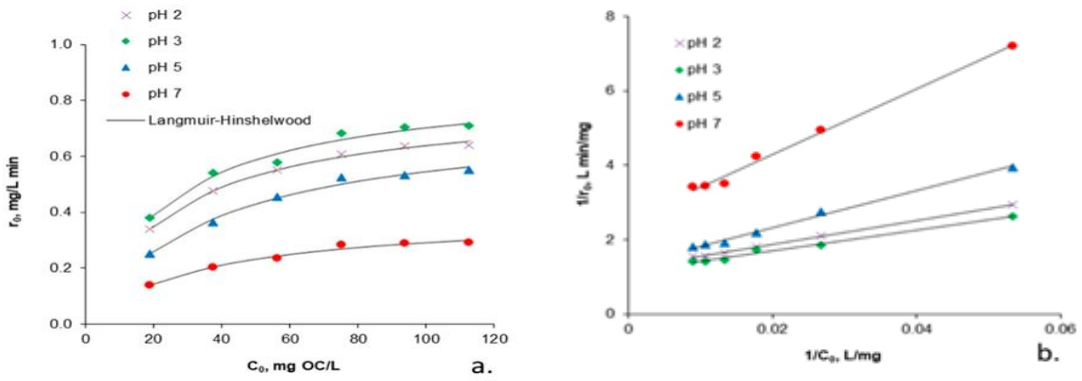

Figure 21. Photocatalytic oxidation kinetics of 2,4-DCF as a function of pH of the working solution: a. non-linear fitting of Langmuir–Hinshelwood kinetics; b. linear fitting of Langmuir–Hinshelwood kinetics; hydrogen peroxide/chlorophenol molar ratio (N) of 1

The data presented in Table 7 shown that the photocatalytic oxidation of 2,4-DCF takes place at a faster rate with the increasing of acidity of the working solution with a maximum corresponding to pH 3.

Table 7. Kinetic parameters derived from Langmuir–Hinshelwood model for photocatalytic oxidation of 2,4-DCF from aqueous solutions with different pH values; hydrogen peroxide/chlorophenol molar ratio (N) of 1

pH	k (mg/L•min)	K (L/mg)
2	0.804	0.039
3	0.872	0.041
5	0.748	0.029
7	0.393	0.027

The rate constant of the photocatalytic oxidation process (k) is about twice as high at pH 3 comparative with pH 7, and the adsorption constant (K) is about 1.4 times higher at pH 3 compared to that corresponding to pH 7. These results are consistent with the results obtained in the adsorption study in the absence of UV radiation (dark adsorption experiments), which confirms that at low pH values of the working solution the adsorption capacity of the catalyst is higher.

Figure 22 shows that the complete mineralization of 2,4-dichlorophenol at an initial concentration of 34.6 mg/L is reached after about 4 h if the working solution has a pH of 3 and after 6 h if the working solution has a pH of 7. If the working solution has a concentration of 112.5 mg/L the time required for complete mineralization of the organic substrate exceeds 9 h in the case of the solution with pH 3 and 17 h in the case of solution with pH 7.

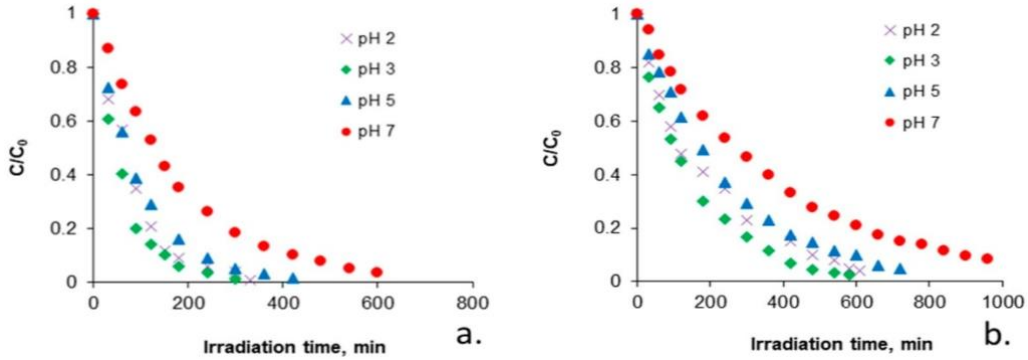

Figure 22. The pH effect on the photocatalytic degradation of 2,4-DCF: a. 18.75 mg OC/L; b. 112.5 mg OC/L; hydrogen peroxide/chlorophenol molar ratio (N) of 1

IV.5 Partial conclusions

The obtained results in this chapter highlight the importance of operating parameters on the photocatalytic degradation efficiency of 2,4-DCF from aqueous solutions using the TiO_2/stainless steel functionalized material. After the experimental tests, was highlighted that the degradation photocatalytic rate increase in acidic conditions (pH = 3) thus, leading to an increase in the photocatalytic degradation efficiency of 2,4-DCF.

Establishment of an optimal stoichiometric ratio between the amount of H_2O_2 and 2,4-DCF is a parameter with a significant importance in the photocatalytic degradation of this organic compound, such that a decrease or increase above the optimal stoichiometric value leads to a significant decrease in the efficiency of the photocatalytic degradation of 2,4-DCF. The photocatalytic degradation rate decreases concomitantly with the increase of the initial concentration of 2,4-DCF. The result obtained in this study indicate an inversely proportional dependence between the initial concentration of the organic compound and the photocatalytic degradation rate of 2,4-DCF.

This chapter was published as: Bobirică L., Bobirică C., Lupu G.I., Orbeci C., Influence of Operating Parameters on Photocatalytic Oxidation of 2,4-Dichlorofenol in Aqueous Solution by TiO_2/Stainless Steel Photocatalytic Membrane. Applied Sciences 2021, 11(24), 11664

Chapter V – TiO_2/Ti and Co-dopped TiO_2/polymer functionalized materials for the degradation of phenolic organic compounds from wastewater

V.1 Specific objectives

In this chapter, the objective was to evaluate the photocatalytic activity of some functionalized materials, such as TiO_2/Ti and Co-doped TiO_2/polymer in the study of the photocatalytic degradation of phenolic compounds. The two functionalized materials were used in the study of the photocatalytic degradation of 4-chlorophenol and 2,4-dichlorophenol.

V.2 Materials and methods

The target organic compounds used in this study were 4-chlorophenol and 2,4-dichlorophenol, in crystalline powder form. The photocatalytic degradation process was realized by monitoring the changes in the concentration of both chlorophenols and antibiotics, also called as organic substrate, as a function of irradiation time by chemical oxygen demand analysis.

A molar ratio of H_2O_2/organic substrate of 1.5 was used throughout all experiments, and the pH working solutions was 3. The samples taken from the reactor were contacted with manganese dioxide to decompose the unreacted H_2O_2.

Next, the samples were filtered and analyzed through the standard method of chemical oxygen demand. The experiments were performed by using synthetic solutions of both chlorophenols, with an initial concentration of equivalent to a chemical oxygen demand value of 100 mg O_2/L, 200 mg O_2/L, and 300 mg O_2/L.

The functionalized materials used in this study were supplied by B.I.T. s.r.l (Milan, Italy). These materials were obtained by grafting technique, respectively grafting polymerization. Both materials contain 30% TiO_2.

V.3 Structural and morphological characterization of TiO_2/Ti and Co-dopped TiO_2/polymer functionalized materials

In figure 26 is presented the FTIR spectra for the functionalized material TiO_2/Ti.

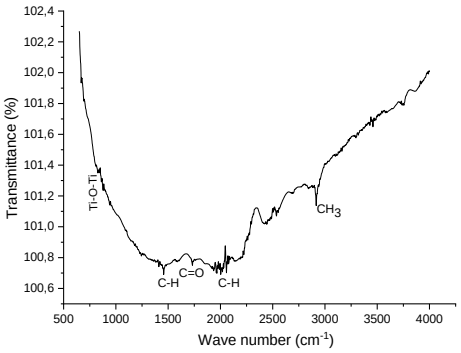

Figure 26. FTIR spectra for TiO_2/Ti

The FTIR spectra for the functionalized material TiO_2/Ti highlight the presence of TiO_2 in the structure of the material.

The peak value of about 826 cm^{-1} can be attributed to the bond Ti-O-Ti. The group corresponding to the value of approximately 1730 cm^{-1} can be attributed to the double bond C=O, and the presence of C-H bond cand be attributed to a peak value about 1457 cm^{-1} and 2003 cm^{-1}. The presence of CH_3 bond cand be attributed to a peak value of approximately 2914 cm^{-1}. The presence of this chemical groups can be attributed to organic residues existing on the surface of the functionalized material, after the photocatalytic degradation of the organic substrate.

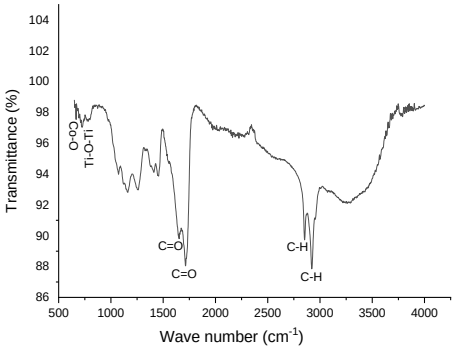

Figure 27. FTIR spectra for Co-doped TiO_2/polymer

The presence of the Co-O bond is shown at a peak value of about 667 cm^{-1}. The values The values of approximately 2850 cm^{-1} and 2919 cm^{-1} can be attributed to the presence of C-H simple bonds, and the presence of C=O bonds is indicated at a peak value of about 1650 cm^{-1} and 1713 cm^{-1}. The presence of this chemical groups can be attributed to organic residues existing on the surface of the functionalized material, after the photocatalytic degradation of the organic substrate. The presence of Ti-O-Ti bond can be attributed to a peak value of about 724 cm^{-1}.

Both functionalized materials TiO_2/Ti and Co-doped TiO_2/polymer were morphological characterized, and the results are presented in figure 28 and figure 29.

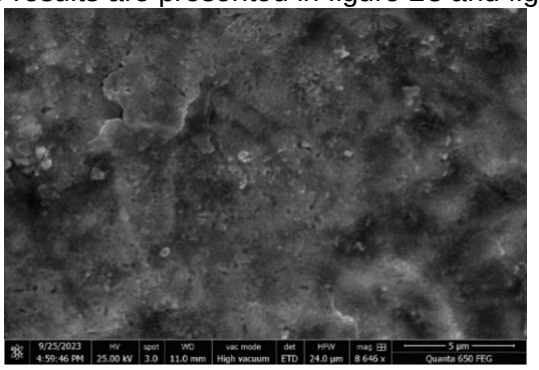

Figure 28. SEM image for TiO_2/Ti

The SEM image corresponding to the functionalized material TiO_2/Ti indicates the presence of TiO_2 particles in its structure. These particles appear uniformly distributed in the material and partially embedded in this support material, most likely due to the TiO_2 deposition process by hot grafting.

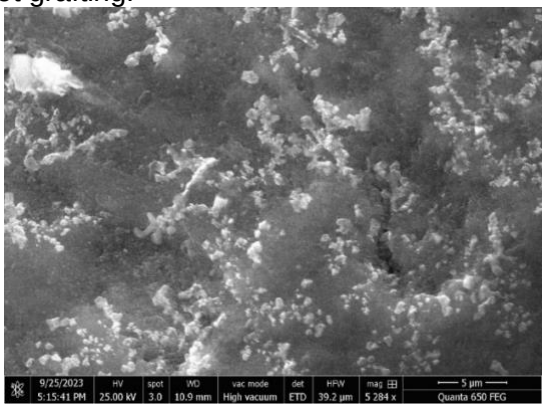

Figure 29. SEM image for Co-doped TiO_2/polymer

The SEM image corresponding to the functionalized material Co-doped TiO_2/polymer indicates the presence of TiO_2 particles in the structure of the polymer support. These particles appear to be uniformly distributed in the polymer material and partially embedded in this material, so this deposition can be observed, only the density of Co-doped TiO_2 is higher at the surface of the polymer material. The TiO_2 particles tend to agglomerate in certain areas

on the surface of the material, probably being the result of the grating-precipitation process, through which the photocatalyst was deposited on the polymeric material used as a support.

V.4 Testing of prepared materials in the study of photo-oxidative degradation of 4-CF and 2,4-DCF

In figures 30-32 are presented the obtained results in the evaluation of the photocatalytic activity of the two functionalized materials prepared.

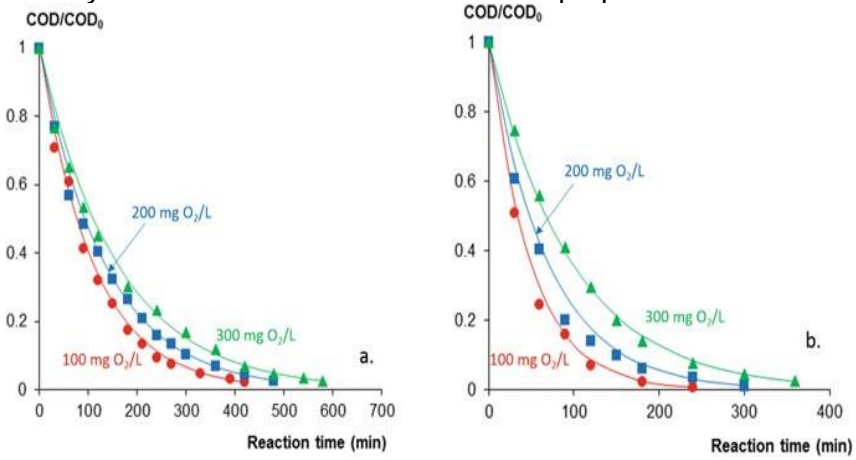

Figure 30. Kinetics of 4-chlorophenol degradation as a function of its initial concentration; a. 4-chlorophenol/H_2O_2=1.5, pH=3, TiO_2/Ti;
b. 4-chlorophenol/H_2O_2=1.5, pH=3, Co-doped TiO_2/polymer

The reaction (irradiation) time until complete mineralization is reached increases with the initial concentration of chlorophenol. The mineralization of aqueous solutions of chlorophenol occurs faster if Co-doped TiO_2/ polymer membrane has been used.

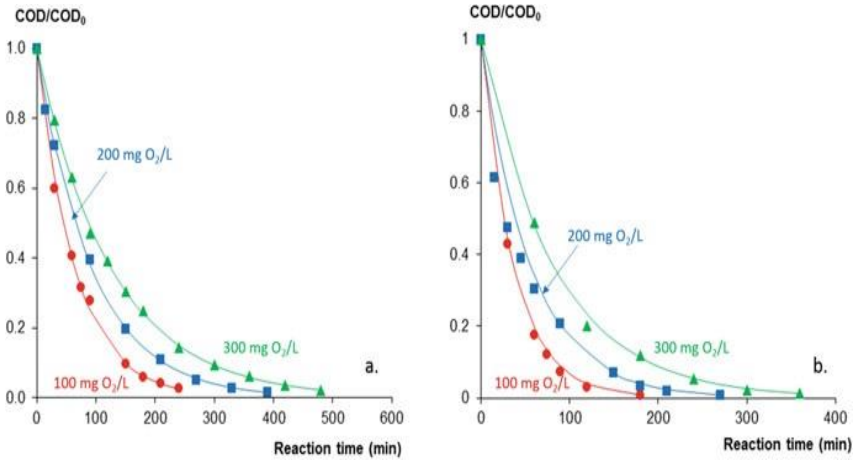

Figure 31. Kinetics of 2,4-chlorophenol degradation as a function of its initial concentration;
a. 2,4- chlorophenol/H_2O_2=1.5, pH=3, TiO_2/Ti;
b. 2,4-chlorophenol/H2O2=1.5, pH=3, Co-doped TiO_2/polymer

The rate of mineralization of 2,4-dichlorophenol aqueous solution depends on the initial concentration of chlorophenol and on the photocatalytic membrane used. Increasing the initial concentration of chlorophenol leads to an increase in irradiation time until complete mineralization. Also, the use of Co-doped TiO_2/polymer increases the mineralization rate.

where: COD, chemical oxygen demand at reaction time, t;

COD_0, initial chemical oxygen demand.

As shown in figures 30 and 31, the reaction time to complete mineralization increases simultaneously with the increase in the concentration of chlorophenol in the initial solution, regardless of the type of chlorophenol and the photocatalytic membrane used.

The obtained results can be explained by the fact that between the initial concentration of the organic substrate and the reaction rate, there is an inversely proportional dependence, so that the higher the initial concentration of chlorophenol, the lower the overall reaction rate. The explanation is that at constant light intensities and irradiation times, as the initial concentration of chlorophenol increases, more and more organic molecules are

adsorbed on the surface of the TiO_2 photocatalyst, while the number of HO• radicals formed on its surface remains constant. This fact causes a decrease in the ratio of the number of HO• radicals and the number of organic molecules, which is reflected in lower degradation efficiencies.

Regarding the photocatalytic efficiency of the studied functionalized materials, in figure 30 and figure 31, it can be observed that the rate of photocatalytic degradation is higher in the case of Co-doped TiO_2/polymer than that of TiO_2/Ti for both 4-chlorophenol and 2,4-dichlorophenol. These results can be explained by the fact that doping the transition metal cobalt (Co) into TiO_2 lattice leads to obtaining a narrow band gap due to the spin exchange interactions which leads the enhancement of photocatalytic activity.

V.5 Partial conclusions

The two phenolic compounds were degraded with significantly high efficiencies using the two photocatalytic membranes. The obtained experimental results in this research chapter regarding the photocatalytic degradation of this phenolic compounds showed that the degradation efficiency of 4-chlorophenol is higher than that of 2,4-dichlorophenol. Using the Co-doped TiO_2/polymer, significantly high photocatalytic degradation efficiencies were obtained. The degradation rate of 4-chlorphenol and 2,4-dichlorophenol is higher for the Co-doped TiO_2/polymer membrane than that of TiO_2/Ti.

Chapter VI – TiO_2/fiberglass functionalized materials for degradation of pharmaceutical organic compounds from wastewater

VI.1 Specific objectives

In this chapter, the objective was to obtain and to evaluate efficiently photo-oxidative functionalized materials, such as TiO_2/fiberglass, different types of fiberglass such as fiberglass type stratified network, type fabric and type mesh. Testing the efficiency of these obtained functionalized materials was carried out using a pharmaceutical compound of the antibiotic type, namely azithromycin.

VI.2 Materials and methods

- Preparation of synthetic azithromycin solution

Azitrox formulation (200 mg/5 mL powder for oral suspension) from Zentiva was purchased from a human pharmacy and used as an organic compound.

Oral suspension of 15 mL (200 mg azithromycin/5 mL) was prepared according to the prospectus; azithromycin powder was dissolved in 7.5 mL of distilled water, under continuous stirring until a uniform suspension was obtained. From this suspension, were prepared the working solutions, stock solution A and stock solution B.

Stock solution A: a volume of 2.5 mL of the prepared suspension was diluted in a 100 mL volumetric flask.

Stock solution B: a volume of 50mL from stock solution A was diluted in a 2500 mL volumetric flask. After stirring, the solution was left at room temperature for 24 hours to ensure complete dissolution of azithromycin, whose solubility in water is very low.

For the determination of chemical oxygen demand was used the APHA 5220 D standard method, described in chapter IV.

Three series of functionalized materials were synthesized, in three different types (experiment 1, 2, 3), using three types of fiberglass (type stratified network, type fabric and type mesh).

Experiment 1 *(1A, 1B, 1C).* Dip coating in 10% solution SBS (type T166) in chloroform + 1% TiO_2

Experiment 2 *(2A, 2B, 2C).* Pre-treatment in H_2SO_4, dip coating in nano-TiO_2 solution and calcination

Experiment 3 *(3A, 3B, 3C).* Dip coating in nano-TiO_2 solution and calcination

VI.3 Structural and morphological characterization of TiO_2/fiberglass functionalized materials

For the obtained functionalized materials, were realized FTIR analysis and SEM-EDX analysis.

In figure 38 are presented the FTIR spectra for the functionalized materials synthesized in experiment 1.

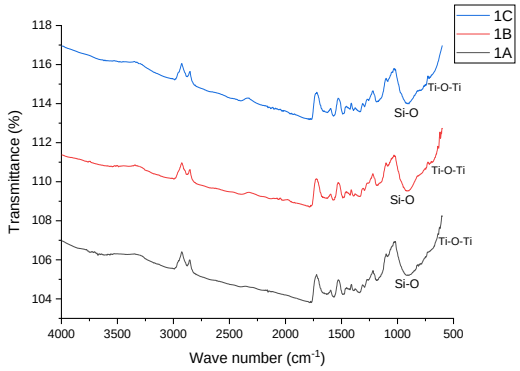

Figure 38. FTIR spectra for the functionalized materials type TiO_2/fiberglass type stratified network, type fabric and type mesh (1A,1B, 1C)

FTIR spectra (figure 38) obtained for all the three functionalized materials obtained in the first experiment indicates a peak value of about 940 cm^{-1} which corresponding to the Si-O bond, specifically to these materials. The presence of TiO_2 is attributed to a peak value of 700-710 cm^{-1} and corresponds to Ti-O-Ti bond.

For the functionalized material namely 1A (TiO_2/fiberglass type stratified network), obtained in the first experiment, the SEM images of the fiberglass indicate a fascicle type

organization of fiberglass, each fascicle being formed from several long and straight fibers arranged in parallel. The size of the TiO_2 particles is at the nanometric level, such as it can be observed that the deposition of TiO_2 is not entirely uniform over the entire surface, in some places smaller or larger particles are visible. In figure 39 are presented the SEM images for the functionalized material TiO_2/fiberglass type stratified network (1A).

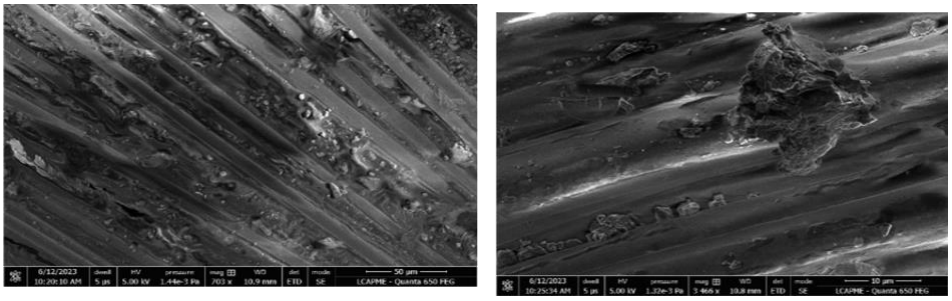

Figure 39. SEM images for the functionalized material 1A (TiO_2/fiberglass type stratified network)

SEM images (figure 41) for the functionalized material 1B (TiO_2/fiberglass type fabric) indicate a morphology like that of the support material, so the presence of the TiO_2 layer on the surface of the fiberglass is relatively small, in some places absent.

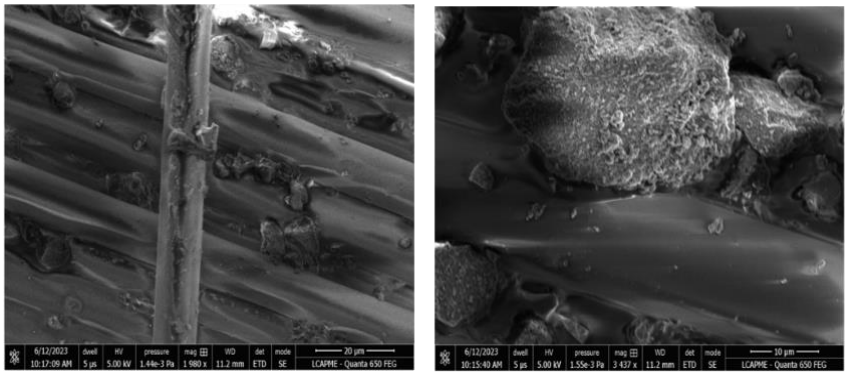

Figure 41. SEM images of the functionalized material 1B (TiO_2/fiberglass type fabric)

For the functionalized material 1C (TiO_2/fiberglass type mesh), SEM images indicate both the parallel arrangement of the fiberglass and the very low presence of the titanium dioxide layer, relatively uniformly deposited on the surface of the support material.

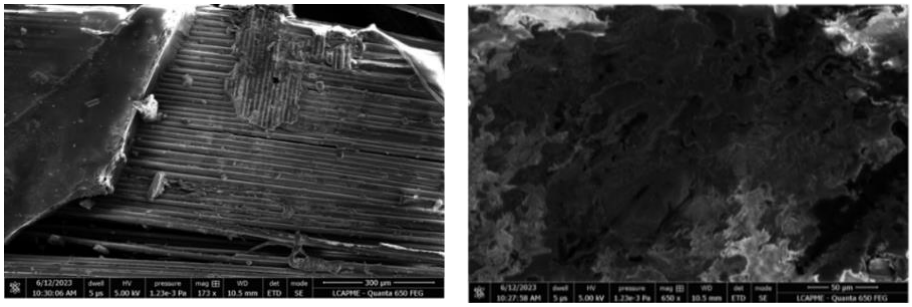

Figure 43. SEM images for the functionalized material 1C (TiO_2/fiberglass type mesh)

Also, for the second series of functionalized materials obtained (experiment 2), were realized analysis for the structural and morphological characterization. In figure 45 are presented the FTIR spectra obtained for the functionalized materials (TiO_2/fiberglass type stratified network, type fabric and type mesh).

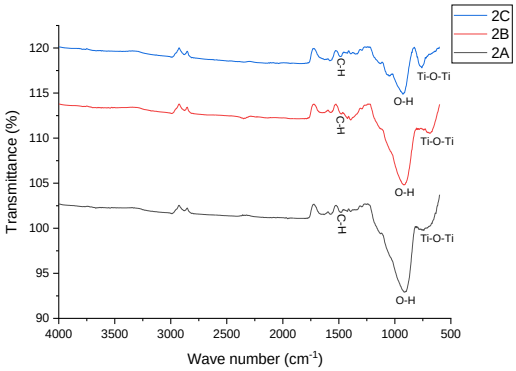

Figure 45. FTIR spectra for the functionalized materials TiO_2/fiberglass type stratified network, type fabric and type mesh (2A, 2B, 2C)

FTIR spectra indicates a peak value included in the interval of about 900-930 cm^{-1} corresponding to C-H bond, and peak value of approximately 1490 cm^{-1} which are corresponding to the presence of C-H bond. Also, a peak value of approximately 750 cm^{-1} can be attributed to the presence of Ti-O-Ti bond.

For the functionalized material 2A (TiO_2/fiberglass type stratified network), the SEM images indicate a similar morphology with the support material, so that on the surface of the fiberglass the presence of TiO_2 layer is insignificant. The increase in the magnitude of the SEM images indicates that the deposition of TiO_2 is not a uniform deposition.

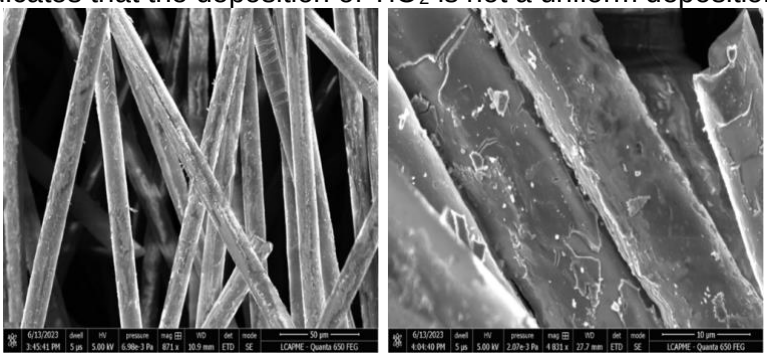

Figure 46. SEM images for the functionalized material 2A (TiO_2/fiberglass type stratified network)

SEM images obtained for the functionalized material 2B (TiO_2/ fiberglass type fabric) indicates a parallel arrangement of fiberglass, Ti particles being also present, thus certifying the deposition of the TiO_2 layer. An increase of magnitude of SEM images indicates that the TiO_2 deposition is non-uniform.

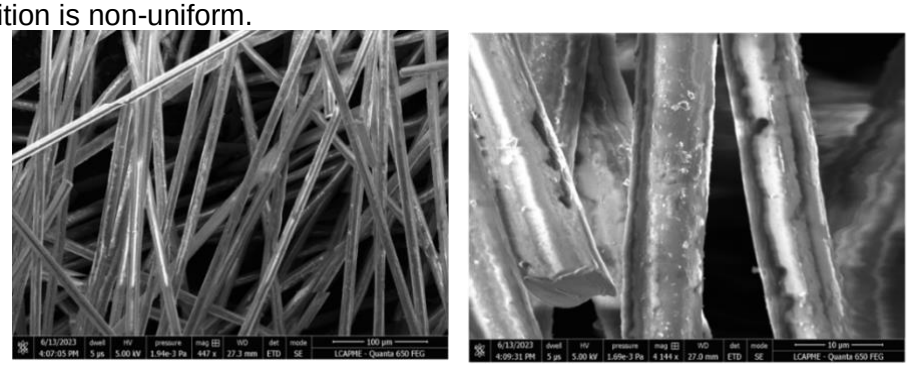

Figure 48. SEM images of the functionalized material 2B (TiO_2/fiberglass type fabric)

SEM images of the functionalized material 2C indicates the presence of TiO_2, but also the parallel structure of the long, straight strands of the mesh-like fiberglass on which the titanium dioxide has been deposited.

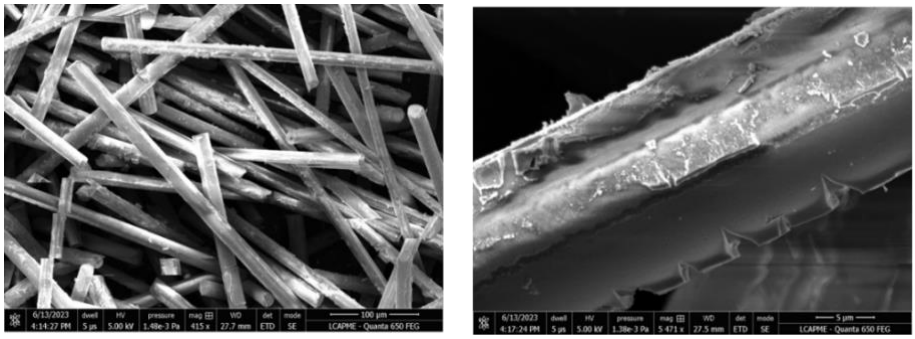

Figure 50. SEM images for the functionalized material 2C (TiO_2/fiberglass type mesh)

In figure 52 are presented the FTIR spectra for all the three functionalized materials. At peak value of about 920 cm^{-1} is indicate the presence of O-H chemical bond; at another peak values of approximately 1480-1496 cm^{-1} are indicate the presence of C-H bond, and the presence of double bond C=O is attributed to a peak value of about 1570 cm^{-1}. The presence of TiO_2 can be attributed to a peak value of about 760 cm^{-1} which cand be attributed to the presence of Ti-O-Ti bond.

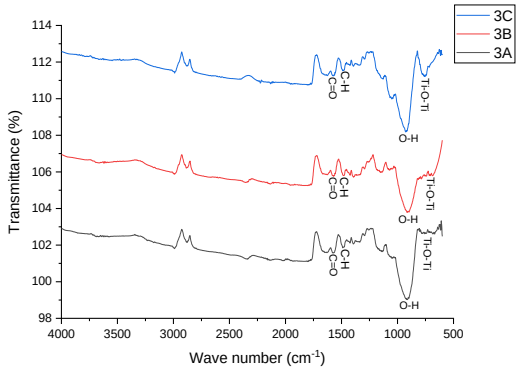

Figure 52. FTIR spectra for the functionalized material TiO_2/fiberglass type stratified network, type fabric and type mesh (3A, 3B, 3C)

The SEM images for the fiberglass type stratified network indicate a parallel arrangement of long glass threads, but also the presence of Ti particles on the surface of support material.

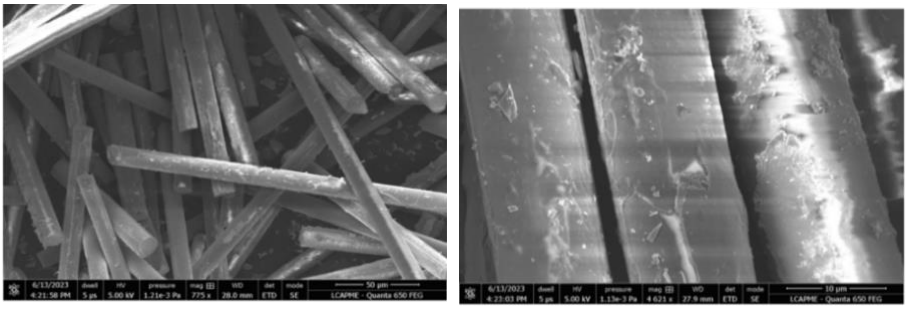

Figure 53. SEM images for the functionalized material 3A (TiO_2/fiberglass type stratified network)

In the SEM images obtained for the functionalized material 3B, can be observed the presence of Ti particles, suggesting its uneven deposition on the surface of the support material.

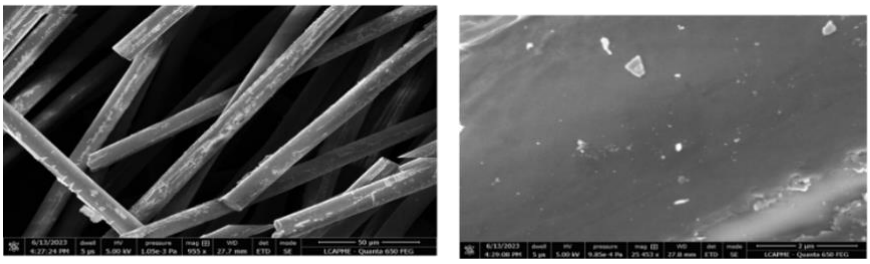

Figure 55. SEM images of the functionalized material 3B (TiO_2/fiberglass type fabric)

The SEM images obtained for the functionalized material 3C (TiO_2/fiberglass type mesh) indicate a parallel disposition of the fiberglass threads and the presence of Ti confirming a controlled and uniform deposition of titanium dioxide.

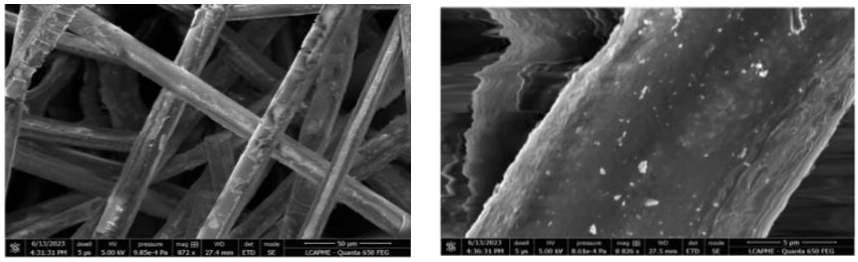

Figure 57. SEM images for the functionalized material 3C (TiO_2/fiberglass type mesh)

VI.4 Testing of TiO_2/fiberglass functionalized materials in the study of photo-oxidative degradation of azithromycin

All the prepared functionalized materials were tested in the study of photocatalytic oxidation of azithromycin. For the functionalized materials namely 1A, 1B, 1C the results are presented in figures 60-62.

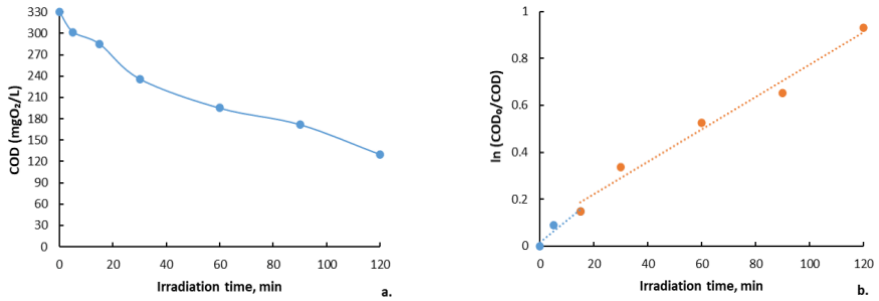

Figure 60. Kinetics of the photocatalytic degradation of the organic content of the azithromycin using the 1A functionalized material: a. COD values against time;

b. $\ln(COD_0/COD)$ against time illustrating pseudo-first-order photocatalytic reaction

The results presented in figure 60 indicate a faster degradation of azithromycin content in the first 30 minutes of irradiation, and further the reaction proceeds slowly until the end of the irradiation time (120 minutes).

Next, in figure 61 are presented the results of the photocatalytic degradation tests for the functionalized material 1B.

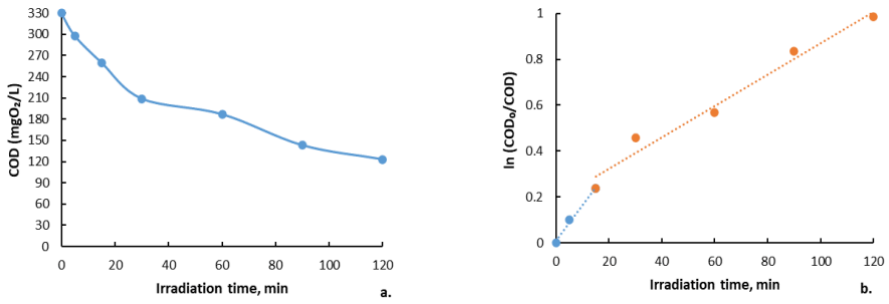

Figure 61. Kinetics of the photocatalytic degradation of the organic content of the azithromycin using the 1B functionalized material: a. COD values against time; b. ln(COD_0/COD) against time illustrating pseudo-first-order photocatalytic reaction

The obtained results for the functionalized material 1B indicate a faster photocatalytic degradation of the organic content (azithromycin) in the first stage of irradiation (0-30 minutes) and a slow degradation in next irradiation time (30-120 minutes). The photocatalytic degradation of azithromycin follows a pseudo-first-order kinetic.

Figure 62 presents the obtained results in the study of photocatalytic oxidation of azithromycin using the functionalized material namely 1C.

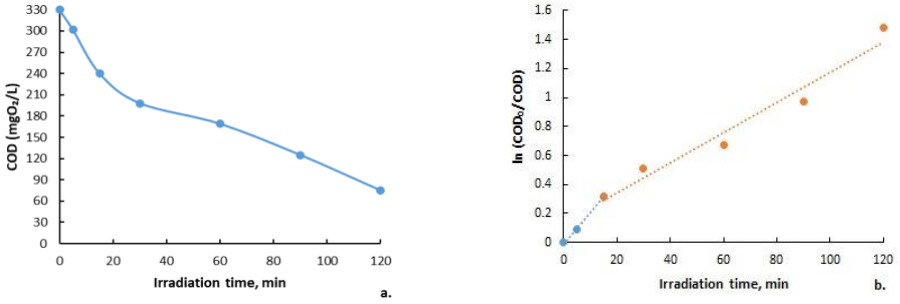

Figure 62. Kinetics of the photocatalytic degradation of the organic content of the azithromycin using the 1C functionalized material: a. COD values against time; b. ln(COD_0/COD) against time illustrating pseudo-first-order photocatalytic reaction

The obtained results indicate that the degradation occurs more rapidly in the first minutes of irradiation (0-30 minutes), and then proceeds more slowly (30-120 minutes), follows a pseudo-first-order degradation kinetic.

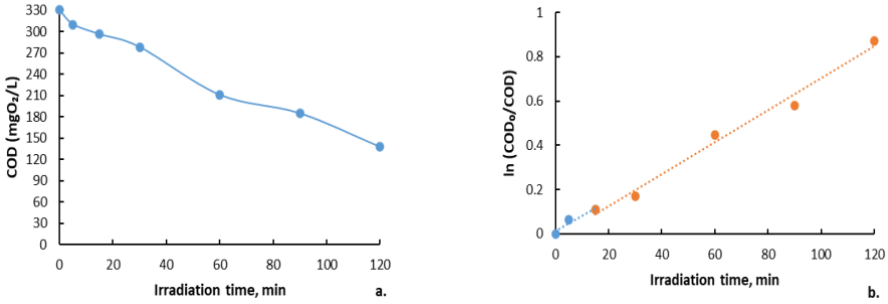

Figure 64. Kinetics of the photocatalytic degradation of the organic content of the azithromycin using the 2A functionalized material: a. COD values against time; b. ln(COD_0/COD) against time illustrating pseudo-first-order photocatalytic reaction

The obtained results indicate that the process takes place faster in the first part of the irradiation time (0-30 minutes), and in the second part of the irradiation time (30-120 minutes) it takes place more slowly.

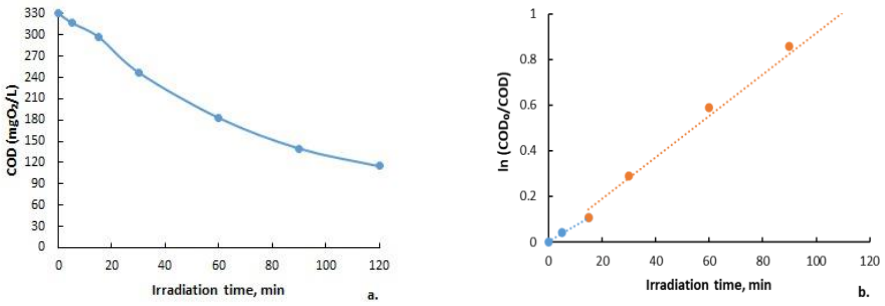

Figure 65. Kinetics of the photocatalytic degradation of the organic content of the azithromycin using the 2B functionalized material: a. COD values against time; b. ln(COD_0/COD) against time illustrating pseudo-first-order photocatalytic reaction

The results obtained in the study of the photocatalytic oxidation of azithromycin, presented in figure 65, indicate a faster photocatalytic degradation of the organic compound of azithromycin in the first minutes of irradiation (0-30 minutes), with a slower reaction rate occurring in the following minutes of irradiation (30-120 minutes).

Figures 67-69 present the results obtained in the study of the photocatalytic oxidation of the organic content of azithromycin using TiO_2/fiberglass functionalized material (3A, 3B, 3C).

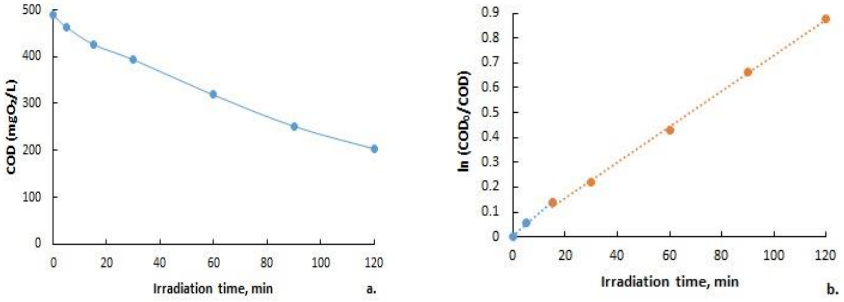

Figure 67. Kinetics of the photocatalytic degradation of the organic content of the azithromycin using the 3A functionalized material: a. COD values against time; b. ln(COD_0/COD) against time illustrating pseudo-first-order photocatalytic reaction

The results in Figure 67 indicate a rapid degradation of the organic compound of azithromycin in the first 30 minutes of UV irradiation, while in the second stage (30-120 minutes) the reaction proceeds at a slower degradation rate, following a pseudo-first-order photocatalytic reaction.

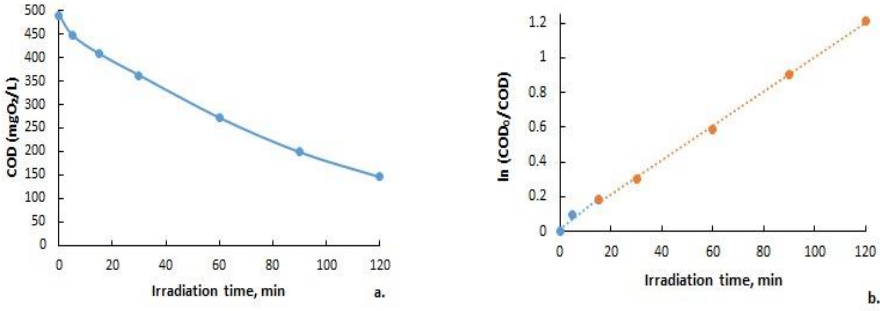

Figure 68. Kinetics of the photocatalytic degradation of the organic content of the azithromycin using the 3B functionalized material: a. COD values against time; b. ln(COD_0/COD) against time illustrating pseudo-first-order photocatalytic reaction

The results obtained in the case of the photocatalytic degradation of the azithromycin content using the TiO_2/fiberglass functionalized material type fabric called 3B indicate that the reaction proceeds faster in the first 30 minutes of irradiation, followed by a slower degradation rate in the next (30-120 minutes), so it can be said that the reaction follows a pseudo-first-order kinetics.

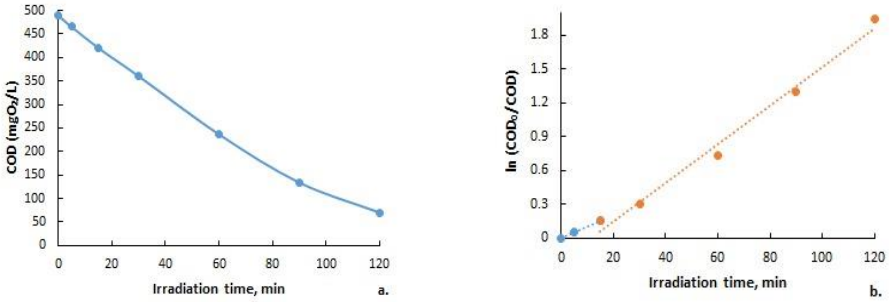

Figure 69. Kinetics of the photocatalytic degradation of the organic content of the azithromycin using the 3C functionalized material: a. COD values against time; b. $\ln(COD_0/COD)$ against time illustrating pseudo-first-order photocatalytic reaction

As can be seen in Figure 69, the photocatalytic degradation of the organic compound of azithromycin in the case of the TiO_2/fiberglass functionalized material type mesh called 3C, the reaction rate is higher in the first 30 minutes of irradiation, followed by a slower degradation rate in the next 30-120 minutes of irradiation. Thus, it can be said that the reaction follows a pseudo-first-order kinetics.

VI.5 Partial conclusions

Based on the characterizations and results obtained from the study of the photocatalytic oxidation of azithromycin using the TiO_2/fiberglass support of functionalized materials of type layered network, type fabric, and type mesh prepared in three different ways, the following conclusions were drawn:

- in the case of the functionalized materials 1A, 1B, and 1C synthesized by immersion coating in a solution of styrene–butadiene–styrene elastomer type T 166 (10% SBS) in chloroform and deposition of photocatalyst (1% TiO_2), the deposition was not uniform over the entire surface of the support material, and the photocatalytic degradation efficiencies of the organic compound of azithromycin reached values between 60-77%, with the highest degradation efficiency being achieved in the case of the use of the functionalized material called 3C (TiO_2/fiberglass support type mesh), reaching a value of approximately 77.2%;
- in the case of the functionalized materials 2A, 2B, and 2C prepared in a first step of pre-treatment with H_2SO_4 followed by immersion coating in a solution of nano-TiO_2 and calcination, it can be stated that due to the pre-treatment with H_2SO_4, these functionalized materials presented a fragile character, being easily friable, thus the functionalized material type TiO_2/fiberglass support type mesh (2C) could not be tested in the study of the photocatalytic oxidation of the azithromycin;
- In the case of the functionalized materials 3A, 3B, and 3C, the TiO_2 deposits on the surface of the support material (fiber glass) were uniform, resulting in high photocatalytic degradation efficiencies of up to 85% (in the case of 3C).

Part of this chapter was published as: Giovanina - Iuliana Lupu, Liliana Bobirică, Constantin Bobirică, Cristina Orbeci. Photocatalytic oxidation of azithromycin in aqueous solution by TiO_2-coated fiberglass membrane. UPB Scientific Bulletin Series B: Chemistry and Materials Science 2023, 85(2), 35-4

Chapter VII – TiO_2/fiberglass and Nb-dopped TiO_2/fiberglass functionalized materials

VII.1 Specific objectives

In this chapter, two distinct functionalized materials were synthesized, characterized, and tested in the study of photocatalytic oxidation, namely TiO_2/ fiberglass functionalized materials type stratified**,** noted MI, and TiO_2 doped with Nb/fiberglass type stratified network, denoted MII. Following the results obtained in the previous chapter (chapter VI), it was chosen the inert support of fiberglass type stratified network functionalized materials, with the use of TiO_2 obtained by combustion (350 °C).

VII.2 Materials and methods

In the experimental studies conducted in this chapter, a synthetic solution of azithromycin was used, prepared according to the method described in subchapter VI.2.

The chemical oxygen demand (COD) was determined using the standard APHA 5220 D method (closed-flow, colorimetric method) [105] described in chapter IV.

Samples of 10 mL of solution were taken from the photocatalytic reactor at different irradiation times, namely at 0, 5, 15, 30, 60, 90, and 120 minutes after the UV radiation lamp was turned on.

The most important problem encountered in the formation of photocatalytic materials is to ensure the adhesion of TiO_2 (or another photocatalyst) to the membrane support, while ensuring a very good dispersion on the surface of the material.

Taking into account the nature of the support (fiberglass) and the photocatalytic component (TiO_2 powder), sodium silicate solution was used as a binder.

The reason for using sodium silicate solution as a binder is due to the fact that it is compatible with both the fiberglass support and titanium dioxide, in the sense that sodium silicate can interact with the glass fiber and TiO_2 (forming a hydrated TiO_2 suspension which, by heat treatment, can partially interact with sodium silicate in a basic medium to form mixed oxides).

For the preparation it was used a sodium silicate solution with the following characteristics:

- SiO_2 content – 36.22%;
- Na_2O content – 12.55%;
- Silicic mode (SiO_2/SiO_2) = 2.98;
- Density – 1.4088 g/cm^3

For the preparation of functionalized materials some stages were completed:

- Cutout fiberglass support 30x10 (Lxl);
- Dilution of sodium silicate solution/distilled water, in a volumetric ratio of 1/5;
- Mixing of TiO_2 powder with the diluted sodium silicate solution in a mass ratio of 1/10
- Preparation of the fiberglass support material by activating with 5% sodium hydroxide solution for 30 minutes, and then washing with distilled water;
- Forming fiberglass support in a cylindrical shape;
- Immersing the cylindrical fiberglass support in the sodium silicate/TiO_2 solution;
- After immersion the formatted support was drained and draying the oven at a temperature of 105°C for one hour;
- After drying the oven, the formed fiberglass support was visually examined for stiffness and color, and then support was placed on a large glass watch and subjected to calcination at 180°C for two hours;
- After calcination and cooling the obtained material was washed with distilled water and dried at room temperature for 24 hours.

VII.3 Structural and morphological characterization of TiO_2/fiberglass and Nb-dopped TiO_2/fiberglass functionalized materials

In figure 71, the FTIR spectra for the obtained functionalized materials are presented.

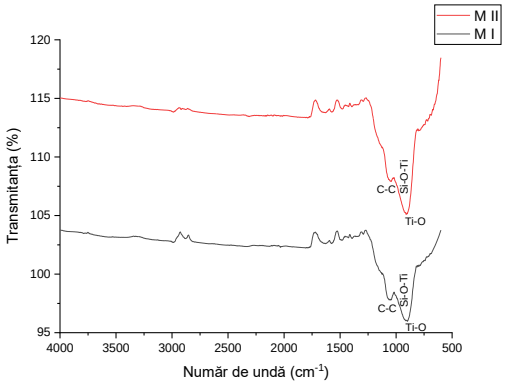

Figure 71. FTIR spectra for the functionalized materials M I and M II

The FTIR spectra for the functionalized material TiO_2/fiberglass namely M I and the functionalized material Nb-dopped TiO_2/fiberglass fiber namely M II presented in figure 71 indicate the presence of the Ti-O bond at peak values of approximately 900 cm^{-1}. The Si-O-Ti chemical bond is present at peak values of approximately 1020 cm^{-1}, and the C-C bond is present at peak values of approximately 1050 cm^{-1}.

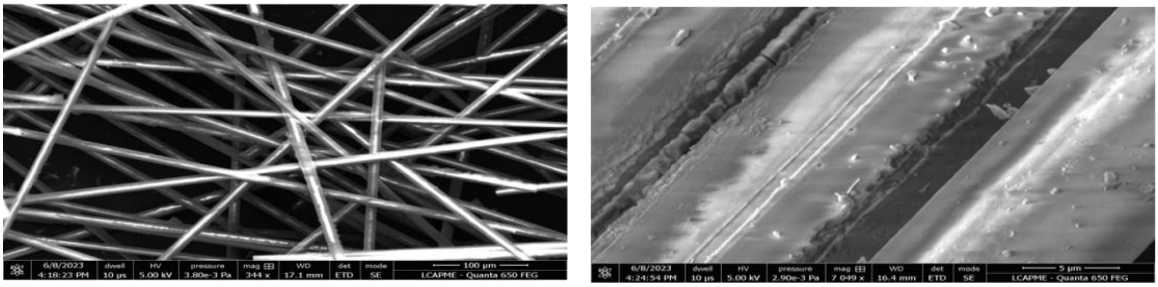

Figure 72. SEM images for the functionalized material TiO_2/ fiberglass type stratified network (M I)

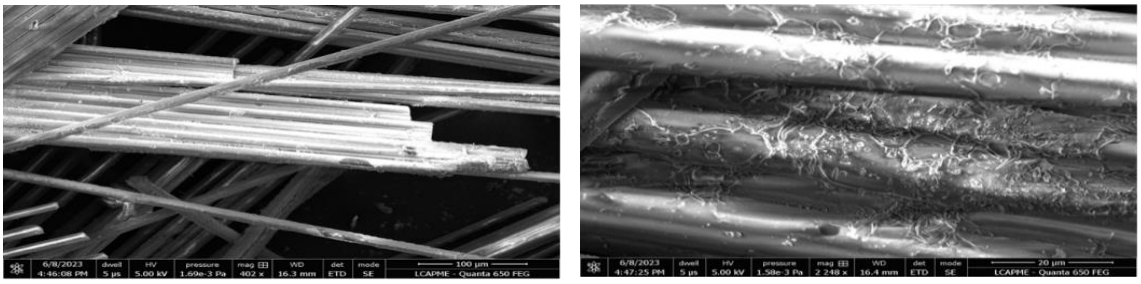

Figure 73. SEM images for the functionalized material Nb-dopped TiO_2/ fiberglass type stratified network (M II)

The SEM images of the functionalized materials type TiO_2/ fiberglass type stratified network and Nb-dopped TiO_2/fiberglass type stratified network indicate a structure of fiberglass type fascicle, each fascicle consisting of several long, straight wires arranged in parallel. The presence of Ti is also visible, with nanometric particle size of 79-282 nm.

VII.4 Testing of prepared functionalized materials in the study of photo-oxidative degradation of azithromycin

In figure 75-76, are presented the results of tested functionalized materials in the study of photo-oxidative degradation of azithromycin.

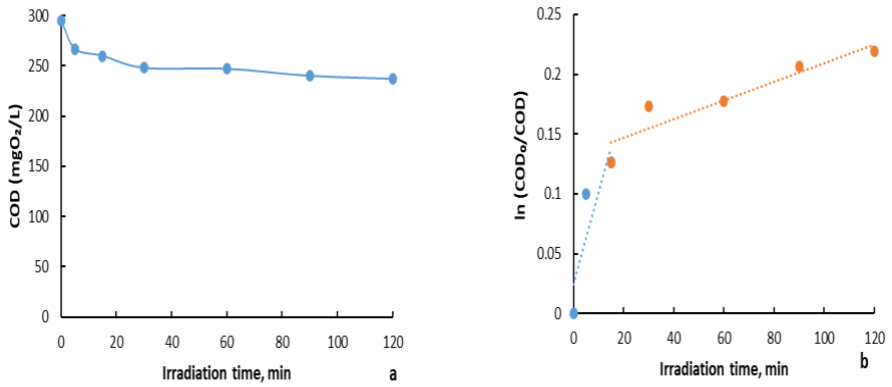

Figure 75. Kinetics of the photocatalytic degradation of the organic content of the azithromycin using the M I functionalized material: a. COD values against time; b. ln(COD_0/COD) against time illustrating pseudo-first-order photocatalytic reaction

As can be observe in the figure 74 and 75 the value of COD decreases proportionally with the increase of the irradiation time.

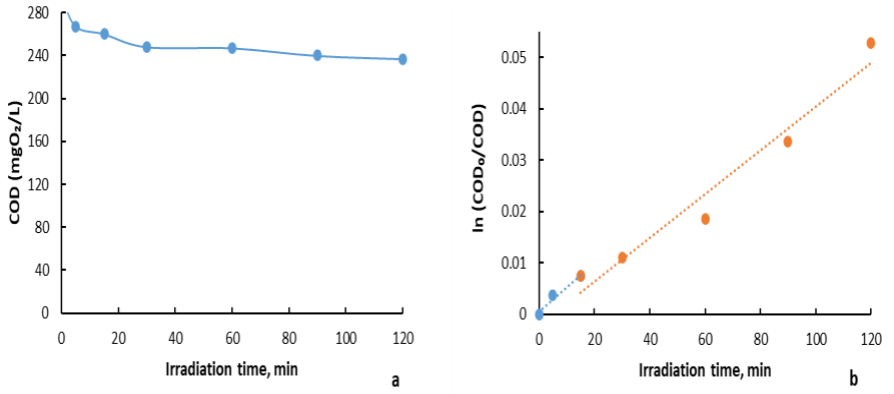

Figure 76. Kinetics of the photocatalytic degradation of the organic content of the azithromycin using the M II functionalized material: a. COD values against time; b. ln(COD_0/COD) against time illustrating pseudo-first-order photocatalytic reaction

Figures 75 and 76 indicate that, for both the functionalized materials M I and M II, the photocatalytic degradation process of azithromycin proceeds with a higher reaction rate in the first 30 minutes, and then the reaction rate decreases significantly, without changes in COD values.

VII.5 Partial conclusions

For the functionalized materials TiO_2/fiberglass and Nb-doped TiO_2/fiberglass, using sodium silicate as a binder, the degradation efficiencies reached values of approximately 24.5% in the case of M I and only 5.4% in the case of M II. The low values of these degradation efficiencies confirm that the deposition of the photocatalyst was not uniform, hence the lack of photocatalytic activity of these materials, and the impossibility of using them in the photocatalytic degradation processes of azithromycin antibiotics.

Chapter VIII – Nb-dopped TiO_2/fiberglass and Nb and $FeCl_3$-dopped TiO_2/fiberglass functionalized materials

VIII.1 Specific objectives

The objectives of the study presented in this chapter were the development of new functionalized materials such as Nb-dopped TiO_2/fiberglass type mesh and Nb and $FeCl_3$-dopped TiO_2/fiberglass for the photo-oxidative degradation of the antibiotic azithromycin from synthetic solutions. In the first step, Nb-doped TiO_2 and Nb and Fe-doped TiO_2 photocatalysts were prepared by the solution combustion synthesis method, and then they were structurally and morphologically characterized. In the second step, the thus prepared photocatalysts were manually embedded on an inert glass fiber mesh support using a polymeric material, namely polydimethylsiloxane (PDMS) as a binder. The functionalized materials thus prepared were subjected to structural and morphological characterization, and then tested in the photo-oxidative degradation study of azithromycin.

VIII.2 Materials and methods

In the experimental studies carried out in this chapter, synthetic azithromycin solution prepared according to the method described in subchapter VI.2 was used.

To determine the chemical oxygen consumption, the standard method APHA 5220 D (closed flow, colorimetric method) [105] described in chapter IV was used.

Samples of 10 mL of solution were taken from the photocatalytic reactor at various irradiation times, namely at 0, 5, 15, 30, 60, 90, and respectively at 120 min from the start of the UV radiation lamp.

For the preparation of Nb-doped TiO_2 and Nb- and Fe-doped TiO_2 photocatalysts, a series of chemical reagents were used such as: Ti(IV) iso-propoxide, purchased from Sigma Aldrich; nitric acid, purchased from Sigma Aldrich and glycine ($C_2H_5NO_2$), purchased from Carl Roth.

In the preparation of niobium and/or iron co-dopped (15% Nb) or undoped TiO_2, the chemicals, Ti(IV) iso-propoxide (Sigma Aldrich), nitric acid (Sigma Aldrich) and glycine (Carl Roth), were used without further purification. The oxidant titanyl nitrate was prepared by slow hydrolysis of 9 mL Ti(IV) iso-propoxide added drop wise under vigorous stirring in 30 mL followed by nitration with 4 mL of nitric acid under ice cold conditions and vigorous stirring for 3h. The titanylnitrate obtained was mixed with glycine (2.4 g), ammonium niobate (V) oxalate 103 hydrate (Sigma Aldrich) (1.17 g) and iron (III) chloride hexahydrate (Sigma Aldrich) (0.1 or 0.2 g) for 1h under stirring. After thorough mixing, the resulting solution was kept in furnace at 773K for 1h. For comparison, 15% Nb-TiO_2 and TiO_2 (were synthesized in accordance with the procedure, but without addition of ammonium niobate (V) oxalate hydrate and/or iron (III) chloride hexahydrate in solution.

The photocatalysts thus prepared were further named as: P1 (TiO_2 doped with 15% Nb), P2 (TiO_2 doped with Nb 15% and Fe 0.1 g) and P3 (TiO_2 doped with Nb 15% and Fe 0.2 g).

The functionalized materials were made from an inert fiberglass support on which a layer of rubberized silicone (PDMS) was deposited, in which the photocatalyst was previously added namely, Nb-TiO_2 and Nb-Fe-TiO_2. In this respect, to develop the membrane, the fiberglass membrane was immersed in a homogeneous mixture of rubberized silicone (PDMS) and photocatalysts at a mass ratio of rubberized silicone/titanium dioxide of 5/1, the mixture was mixed and then, it was deposited on the fiberglass surface. Next, the obtained photocatalytic membrane was dried at room temperature for 24 hours.

Thus, three functionalized photocatalytic membrane type materials were prepared:

- 15% Nb-dopped TiO_2 namely M1;
- 15% Nb and Fe (0.1 g)-dopped TiO_2 namely M2;

- 15% Nb and Fe (0.2 g)-dopped TiO_2 namely M3

VIII.3 Structural and morphological characterization of Nb-dopped TiO_2/fiberglass type mesh and Nb and $FeCl_3$-dopped TiO_2/fiberglass type mesh functionalized materials

For to investigate the morphology of the photocatalysts and the morphology of functionalized materials was used a Quanta 650 120 FEG scanning electron microscope (SEM) equipped with EDX analyzer operated at 10 kV.

FTIR analysis was performed on an ATR-FTIR spectrum 100 (PerkinElmer) with 4 consecutive scans in the 4000-550 cm^{-1} region and 4 cm^{-1} resolution. The presented spectra are the average of these scans.

X-ray Photoelectron Spectroscopy (XPS) was performed by using a K-Alpha instrument (Thermo Scientific) with a monochromate Al Kα source which offer photons with 1486.6 eV. Binding energies were calibrated by placing the C 1s peak at 284.4 eV.

In figure 79 are presented the results of SEM-EDX analysis for the photocatalyst 15% Nb-dopped TiO_2.

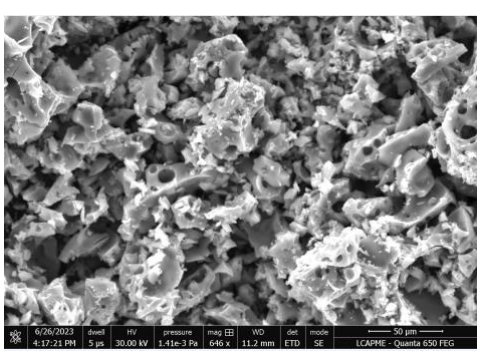

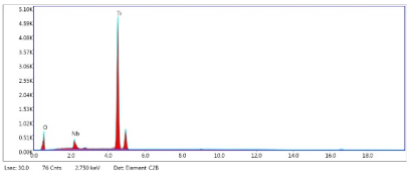

Element	Weight %	Atomic %	Net Int.	Error %	Kratio	Z	A	F
O K	42.67	69.86	151.16	11.51	0.0419	1.1176	0.0877	1.0000
NbL	4.55	1.28	101.52	4.44	0.0378	0.8297	0.9958	1.0037
TiK	52.77	28.86	2042.07	1.23	0.4758	0.9038	0.9935	1.0038

Figure 79. Scanning electron microscopy (SEM) micrographs and energy-dispersive X-ray diffraction (EDX) spectrum for 15%Nb- TiO_2

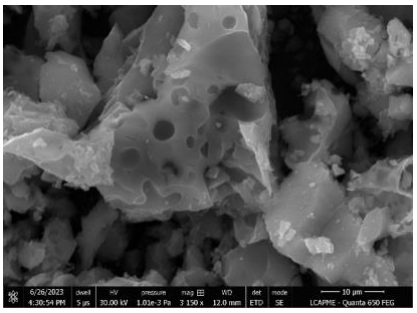

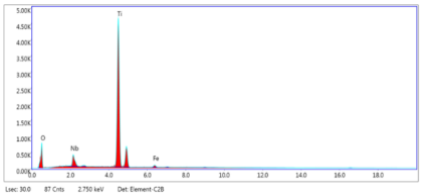

Element	Weight %	Atomic %	Net Int.	Error %	Kratio	Z	A	F
O K	45.29	72.19	181.19	11.30	0.0471	1.1116	0.0936	1.0000
NbL	4.78	1.31	112.80	6.79	0.0394	0.8250	0.9957	1.0035
TiK	48.79	25.98	2000.05	1.26	0.4378	0.8986	0.9927	1.0055
FeK	1.14	0.52	30.69	20.01	0.0093	0.8922	0.8966	1.0207

Figure 80. Scanning electron microscopy (SEM) micrographs and energy-dispersive X-ray diffraction (EDX) spectrum for 15%Nb- TiO_2

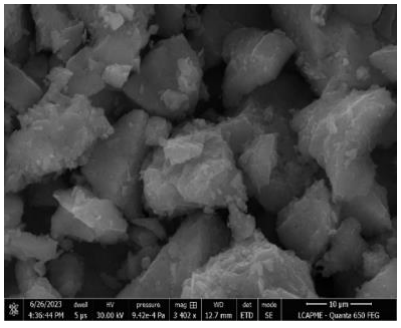

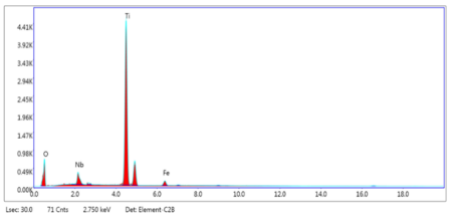

Element	Weight %	Atomic %	Net Int.	Error %	Kratio	Z	A	F
O K	44.07	71.20	170.66	11.35	0.0459	1.1144	0.0935	1.0000
NbL	4.58	1.27	104.03	5.95	0.0376	0.8272	0.9890	1.0035
TiK	48.94	26.41	1944.91	1.26	0.4406	0.9011	0.9924	1.0066
FeK	2.41	1.11	62.76	9.84	0.0197	0.8947	0.8962	1.0196

Figure 81. Scanning electron microscopy (SEM) micrographs and energy -dispersive X-ray diffraction (EDX) spectrum for 15%Nb- TiO_2

As can be seen in the SEM images, there are some agglomerations that are maintained in approximately the same shape and density for all three photocatalysts. The intensity of the peak in the EDX spectra corresponding to Fe increased with the increase of the amount of iron incorporated into the TiO_2 structure, while the intensity of the peak corresponding to Nb is kept constant (EDX spectra in figures 79-81). Therefore, consistent with the XRD analysis, the increase in the amount of iron introduced into the TiO_2 structure suggests the replacement of Ti^{4+} with various iron species.

The SEM images and the EDX spectra obtained for the functionalized materials (M1, M2, M3) are presented in figures 82-84.

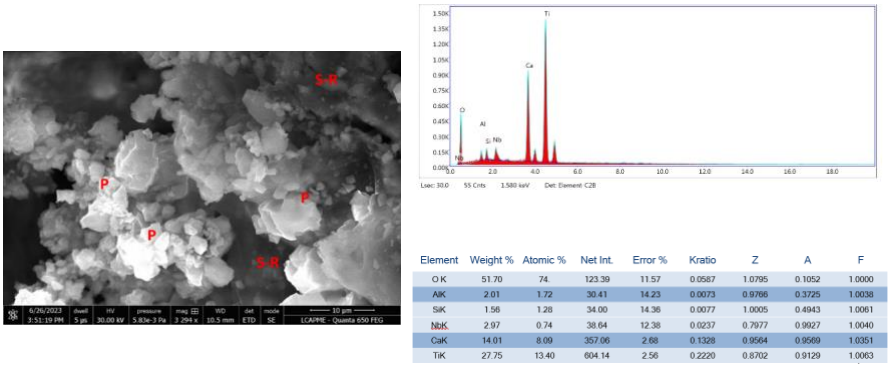

Element	Weight %	Atomic %	Net Int.	Error %	Kratio	Z	A	F
O K	51.70	74	123.39	11.57	0.0587	1.0795	0.1052	1.0000
Al K	2.01	1.72	30.41	14.23	0.0073	0.9766	0.3725	1.0038
Si K	1.56	1.28	34.00	14.36	0.0077	1.0005	0.4943	1.0061
Nb K	2.97	0.74	38.64	12.38	0.0237	0.7977	0.9927	1.0040
Ca K	14.01	8.09	357.06	2.68	0.1328	0.9564	0.9569	1.0351
Ti K	27.75	13.40	604.14	2.56	0.2220	0.8702	0.9129	1.0063

Figure 82. SEM images and EDX spectra for the functionalized materials namely M1

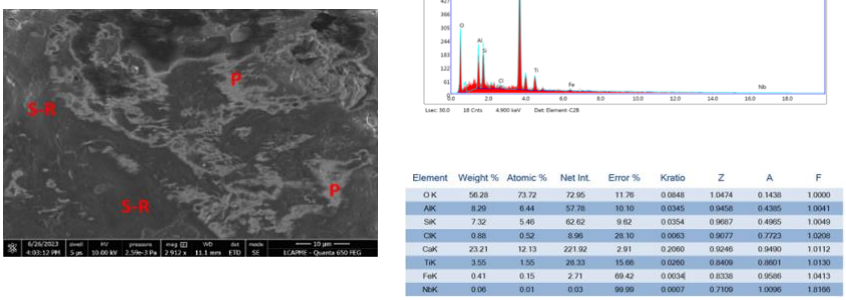

Element	Weight %	Atomic %	Net Int.	Error %	Kratio	Z	A	F
O K	56.28	73.72	72.95	11.76	0.0848	1.0474	0.1438	1.0000
Al K	8.29	6.44	57.78	10.10	0.0345	0.9458	0.4385	1.0041
Si K	7.32	5.46	62.62	9.62	0.0354	0.9667	0.4965	1.0049
Cl K	0.88	0.52	8.96	28.10	0.0063	0.9077	0.7723	1.0208
Ca K	23.21	12.13	221.92	2.91	0.2060	0.9246	0.9490	1.0112
Ti K	3.55	1.55	28.33	15.66	0.0260	0.8409	0.8601	1.0130
Fe K	0.41	0.15	2.71	69.42	0.0034	0.8336	0.9586	1.0413
Nb K	0.06	0.01	0.03	99.99	0.0007	0.7109	1.0096	1.0166

Figure 83. SEM images and EDX spectra for the functionalized materials namely M2

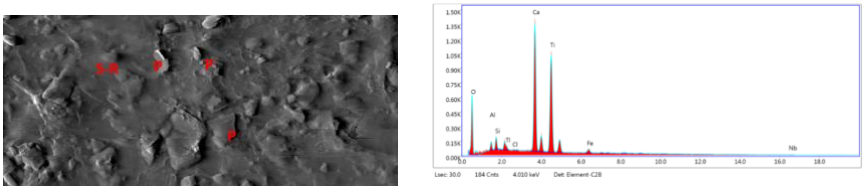

Element	Weight %	Atomic %	Net Int.	Error %	Kratio	Z	A	F
O K	55.38	76.68	155.15	11.27	0.0676	1.0657	0.1146	1.0000
Al K	1.67	1.37	27.48	15.37	0.0061	0.9634	0.3811	1.0034
Si K	1.72	1.36	40.92	13.25	0.0087	0.9869	0.5080	1.0054
Ti K	0.07	0.01	1.08	85.55	0.0009	0.6791	1.4630	1.2773
Cl K	0.04	0.03	1.23	80.51	0.0003	0.9253	0.8245	1.0214
Ca K	19.76	10.92	539.03	2.17	0.1671	0.9426	0.9797	1.0256
Ti K	19.55	9.04	440.27	3.12	0.1510	0.8578	0.8936	1.0083
Fe K	1.03	0.41	17.61	23.16	0.0083	0.8510	0.9292	1.0272
Nb K	0.79	0.19	0.99	83.90	0.0089	0.7273	1.0077	1.5387

Figure 84. SEM images and EDX spectra for the functionalized materials namely M3

As can be seen in figure 82, the photocatalytic membrane M1 shows agglomerations of the photocatalyst (P), which denotes an uneven 230 deposition of it on the surface of the membrane. It seems that, in the case of the M2 and M3 photocatalytic membranes, the photocatalyst is embedded in rubberized silicone/PDMS (S-R), and the distribution of the photocatalyst (P) in the membrane is much more homogeneous than in the case of the M1 photocatalytic membrane.

- Structural characterization of photocatalysts and functionalized materials M1, M2, M3

Figure 85 shows the FTIR spectra for all the three photocatalysts, namely P1, P2 and P3.

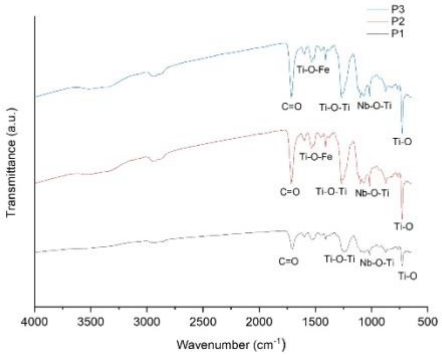

Figure 85. FTIR spectra for the photocatalysts P1, P2 and P3

The presence of some weak transmittance between 700-730 cm^{-1} are attributed to the stretching vibrations of the Ti-O groups. All the three spectra show peaks around 1000 cm^{-1} which could be assigned to Nb-O-Ti vibrations. The transmittance corresponding to 1529 cm^{-1} in P2 and P3 spectra could be attributed to Ti-O-Fe bound [8, 9]. Moreover, the band at approximately 1700 cm^{-1} can be attributed to C=O, most probably derived from the photocatalyst preparation method. Anatase phase of TiO_2 shows certain strong FTIR bands in the region of 1200-1300 cm^{-1}, where is seen the broad intense band attributed to Ti-O-Ti vibrations [10].

The FTIR spectra for all the three functionalized materials are presented in figure 86.

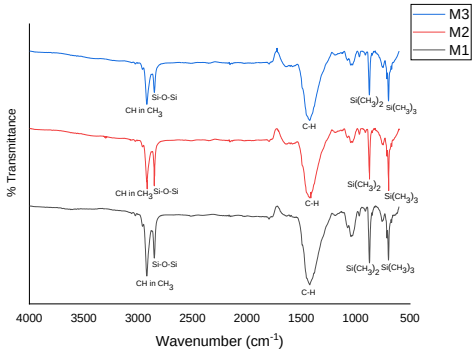

Figure 86. FTIR spectra for the functionalized materials M1, M2 and M3

The peaks at approximately 700 cm^{-1} are corresponding to the functional groups Si-$(CH_3)_3$, and other peaks between 840-790 cm^{-1} can be attributed to Si-$(CH_3)_2$ functional groups. Peaks between 1100-1000 cm^{-1} corresponding to Si-O-Si functional groups [11,12]. All these functional groups show the presence of silicone rubber in the composition of new obtained photocatalytic membranes [13]. Other peaks are at a 2960 cm^{-1} show the presence of CH stretch in CH_3 functional group.

For a thorough structural characterization, XPS analysis was also performed for the three photocatalysts P1, P2 and P3. The XPS spectra are shown in figure 87 a-c.

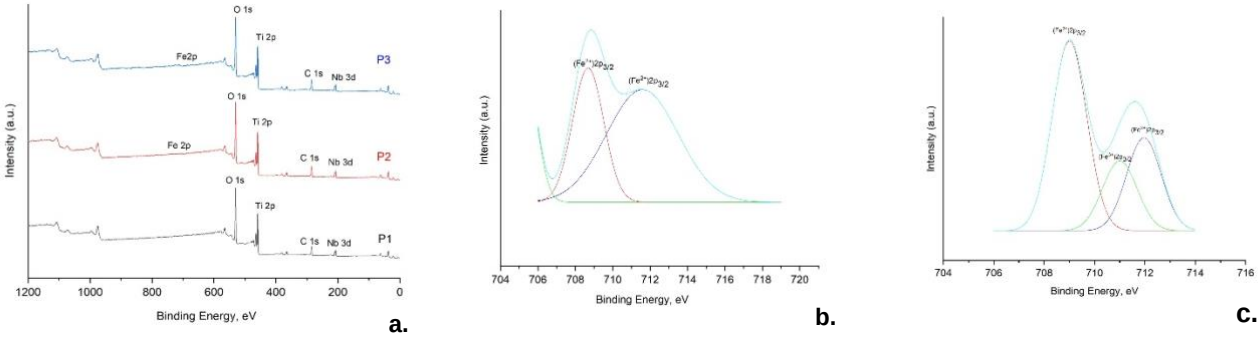

Figure 87. XPS spectra of TiO_2 powders doped with niobium and iron: a. P1, P2, P3; b. Deconvolution of Fe2p spectra in P2; c. Deconvolution of Fe2p spectra in P3.

For the photocatalyst P1, the peaks at 207.35 eV and 458.81 eV are corresponding to Nb 3d (Nb 3d5/2) and Ti 2p (Ti 2p3/2). Nb 3d3/2 peak corresponds to that of Nb^{5+} oxidation state, and Ti 2p3/2 peak corresponds to that of Ti^{4+} oxidation state [14]. For samples P1 and P2, the peaks that appear at approximately 710 eV correspond to the added iron (Fe2p). The deconvolution of these peaks showed that the Fe 2p3/2 peaks correspond to the Fe^{2+} (709 eV) and Fe^{3+} (711 eV and 712 eV) oxidation states. The O 1s peak corresponds to the lattice oxygen of TiO_2.

The XPS analysis was realized for the three functionalized materials M1, M2 and M3. The XPS spectra are presented in figure 88.

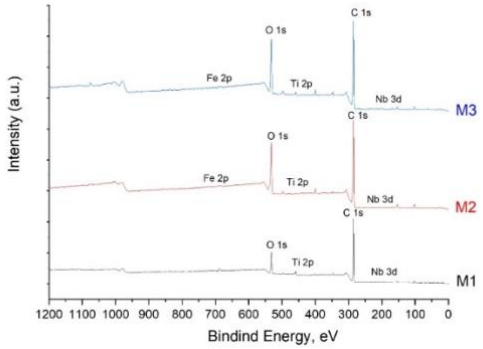

Figure 88. XPS spectra for the functionalized materials M1, M2 and M3

It should be noted that the XPS analysis for the three photocatalytic membranes was performed after the two hours of UV irradiation (after a test cycle of the photocatalytic activity). It seems that the peaks corresponding to titanium (Ti 2p at 458.87 eV,) and niobium (Nb 3d3/2 at 210.27 eV) appear in the spectra of the three photocatalytic membranes, but at a reduced intensity compared to the initial spectra of photocatalysts powders. This denotes a good stability of the photocatalytic membranes, which would allow their use in several successive cycles of photocatalysis. Regarding the peak 201 associated with iron, it is shifted to 219.21 eV corresponding to Fe2p1/2, thus indicating the complete transition to Fe^{3+} in γ-Fe_2O_3 after UV irradiation.

VIII.4 Testing of photocatalytic materials in the study of photo-oxidative degradation of azithromycin

- Photocatalytic initial tests

Initial photocatalytic tests (membrane without added organic material) showed that these photocatalytic membranes are stable, the concentration of organic substrate in solution that could have come from the composition of the membranes was zero. Also, the photocatalyst embedded in the membranes was not released into the solution, which confirms its physical stability.

- Tests of photo-oxidative degradation of azithromycin using the functionalized photocatalytic membrane type materials obtained.

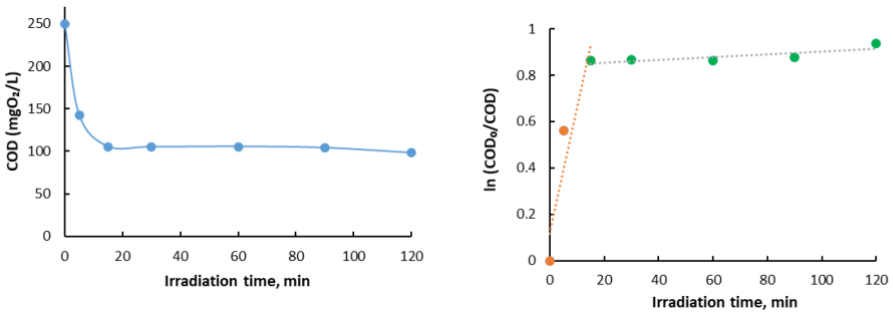

Figure 89. Photocatalytic degradation of azithromycin by using M1: a) variation of the concentration of the organic substrate with the irradiation time; b) pseudo-first-order kinetic model

The results obtained using the M1 membrane (figure 89) indicate a fast degradation of the organic substrate (AZT + excipients) in the first 15 minutes of UV irradiation. The photocatalytic degradation follows a pseudo-first order kinetics whose rate constant over the interval 0-15 minutes is 0.054 min^{-1}. After 15 minutes of UV irradiation, the degradation of the remaining organic substrate continues, but at a very low rate, the rate constant for the interval 15-120 minutes being 0.0006 min^{-1}.

In figure 90 are presented the results on testing M2 in the study of photo-oxidative degradation of azithromycin.

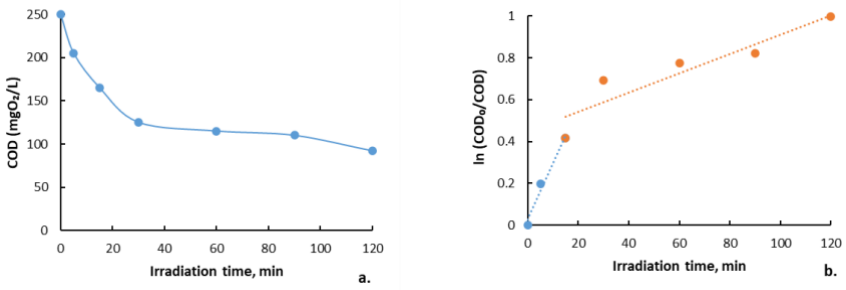

Figure 90. Photocatalytic degradation of azithromycin by using M2: a) variation of the concentration of the organic substrate with the irradiation time; b) pseudo-first-order kinetic model

For M2 photocatalytic membrane (figure 90), the experimental results obtained indicate a good degradation of the organic substrate in the first minutes (0-15 minutes) of the UV irradiation. The process of photocatalytic degradation is following a pseudo-first order kinetics which in the first 15 minutes has a rate constant of 0.0268 min^{-1}. In the next irradiation time (15-120 minutes), the rate constant is 0.0046 min^{-1}.

Figure 91 presents the results obtained in the photocatalytic degradation of azithromycin using M3.

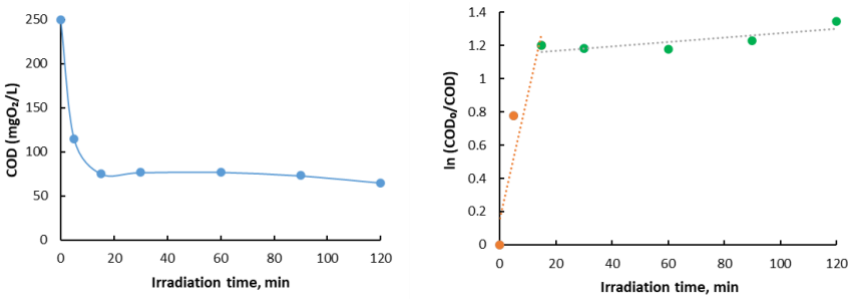

Figure 91. Photocatalytic degradation of azithromycin by using M3: a) variation of the concentration of the organic substrate with the irradiation time; b) pseudo-first-order kinetic model

Regarding the M3 photocatalytic membrane, the degradation kinetics is pseudo-order 1, but the degradation speed is higher than in the case of the M2 membrane. Thus, on the interval 0-15 minutes the rate constant is 0.075 min^{-1}, and on the interval 15-120 minutes the speed constant is 0.0013 min^{-1}. It can be observed that, in all the three cases, the degradation of the organic substrate proceeds in two steps, namely, a first step that proceeds at a high speed over a short irradiation interval and a second sharp step proceeds at a low speed over a long irradiation interval. This could be due to the high rate of degradation of the initial organic substrate to intermediate compounds with greater resistance to the photocatalytic oxidation conditions in the reactor.

VIII.5 Proposed mechanism for the photo-oxidative degradation of azithromycin

Gas chromatography-mass spectrometry (GC-MS) was used to identify the intermediate compounds formed in the photo-oxidative degradation of azithromycin. The gas chromatograph mass spectrometer was a PerkinElmer instrument with Autosystem XL GC, turbo mass MS, autosampler, 2-µL injection, 200° injection port, 200° interface, 70-eV electron impact (EI) mode and 40–630-amu mass range.

To identify the intermediates formed during the photocatalytic oxidation process, an azithromycin solution of 20 mg/L was irradiated, from which samples were taken for approximately 480 minutes (8 hours). The samples were processed to separate and identify the compounds present in them. Thus, based on the chromatograms and mass spectra, both azithromycin (at short irradiation times) and 4 intermediates were identified, the abundance of which changes depending on the irradiation time.

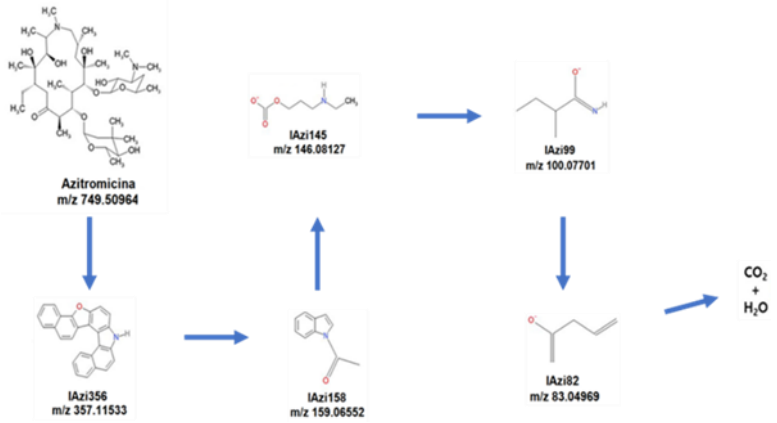

Figure 96. Proposed mechanism of azithromycin mineralization by photocatalytic oxidation

The results presented have indicated that azithromycin breaks down into smaller and smaller molecules until simple compounds under UV irradiation in the experimental conditions of these works, but complete mineralization (when no organic compound was

detected on the chromatograms) is reached at irradiation times of approximately 480 minutes (8 hours).

VIII.6 Partial conclusions

The conclusions resulting from this study are the following:

- modification of the TiO^2 structure by introducing Nb and Fe, an aspect that led to an approximately two-fold increase in its specific surface area;

- this increase determined an easier adsorption of the reactants on the photocatalyst surface, facilitating the photocatalytic degradation process;

- the introduction of Fe into the structure of the photocatalyst led to the triggering of the photo-Fenton degradation mechanism of the organic substrate, which led to the increase of the overall efficiency of the photocatalytic degradation process;

- the fiber glass type mesh/rubberized silicone support in which the photocatalyst was embedded has high mechanical and physicochemical resistance, which gives it the property of being widely used in the synthesis of these types of photocatalytic membranes. Thus, this support has a high elasticity, thus being able to adopt different forms in the photocatalytic reactor, without the risk of losing the photocatalyst from the surface or inside it, being practically inert in strongly oxidizing conditions in the photocatalytic reactor. This type of membranes is of interest for future investigations and for improving their photocatalytic activity.

This chapter will be published as: Giovanina-Iuliana LUPU, Cristina ORBECI, Constantin BOBIRICĂ, Liliana BOBIRICĂ, Elena Sorana LAZĂR, Jeanina PANDELE-CUSU, Marian Nicolae VERZIU, Cristian PÎRVU, Roberta-Geanina IRODIA. Photocatalytic degradation of azithromycin formulation in aqueous solution by doped titanium dioxide/fiberglass-rubberized silicone photocatalytic membrane. Sustainable Environment Research, 2023 *F.I. 4,9*

Chapter IX – Nanocomposite materials based on cellulose acetate and graphene oxide and PTFE coating with TiO_2 covered

IX.1 Specific objectives

In this chapter, the main objective was to develop a novel type of nanocomposite material based on cellulose acetate combined with small amounts of graphene oxide with TiO_2 covered. The specific objectives were to characterize these functionalized materials and to test it in the study of photocatalytic oxidation of azithromycin.

IX.2 Materials and methods

Cellulose acetate (CA), titanium dioxide, and graphene oxide (GO) were purchased from Sigma-Aldrich. N,N′-dimethylformamide (DMF) and ethanol were purchased from Merck with analytical purity and used as such, without any additional purification processes.

Polytetrafluoroethylene (PTFE) rod was used to mechanically machine magnetron targets according to the technical specifications of the magnetron sputtering gun (diameter: 25.4 mm, thickness: 3.18 mm). After preparation, the PTFE targets were cleaned by ultrasonication in ethanol (laboratory grade) before mounting on the magnetron gun.

Azitrox formulation (200 mg/5 ml powder for oral suspension – antibiotic azithromycin) from Zentiva was purchased from a human pharmacy. It contains the active component (azithromycin dihydrate) and a series of organic and inorganic excipients (sugar, trisodium phosphate anhydrous, hydroxypropyl cellulose, xanthan gum, and banana flavour).

In the experimental studies carried out in this chapter, synthetic azithromycin solution prepared according to the method described in subchapter VI.2 was used.

To determine the chemical oxygen consumption, the standard method APHA 5220 D (closed flow, colorimetric method) [105] described in chapter IV was used.

Samples of 10 mL of solution were taken from the photocatalytic reactor at various irradiation times, namely at 0, 5, 15, 30, 60, 90, and respectively at 120 min from the start of the UV radiation lamp.

Functionalized composite materials with embedded graphene oxide and TiO_2 were prepared based on sonochemical and phase inversion methods**.**

The polymer solution was prepared by dissolving the cellulose acetate (CA) in N,N′-dimethylformamide (DMF) at desired concentration (12%) under magnetic stirring for 24 hours at room temperature. For composite membranes preparation, three different concentrations of GO were used, by adding the desired amount of GO in polymer solution at three different concentrations – 0,5%, 1%, 2%, related to polymer mass in solution. Along with graphene, the same amount of TiO_2 was added in every solution.

The coverage of graphene oxide with titanium dioxide and also dispersion of covered nanofiller in the polymer solution were performed under sonication for 30 minutes and cooled on an ice bath in order to keep the temperature below 5°C.

After 30 min sonication, a homogeneous, slightly viscous, and black mass was obtained. Membrane obtaining was accomplished by depositing polymer solution onto a spectral glass having a blade fixed at a standard thickness of 250 μm.

The formed polymer solution films were then immersed in the coagulation bath containing 200 mL of distilled water and after synthesis the obtained membranes were washed consequently with deionized water and ethanol.

The deposition of PTFE films was conducted in a spherical stainless-steel vacuum chamber, equipped with a 1 inch magnetron sputtering source. The PTFE sputtering deposition process was performed by operating the discharge using an RF power generator (13.56 MHz) with 80 W in argon (purity 99.9999%), at 100 sccm flow rate, which established a working pressure of 1.4×10^{-3} mbar.

For the poisoning prevention of the targets, the magnetron source was technical adjusted by mounting a chimney just in front of the magnetron ring.

For obtaining composite membranes with improved mechanical and chemical properties the sputtering time was set for 50 minutes for 200 nm thickness of the PTFE layers onto the face oriented towards the UV radiation and just 5 minutes (20 nm) on the opposite face, just to ensure its hydrophobization.

Chemical structure of the CA/GO support membranes and PTFE/CA-GO composite membranes was investigated by Fourier Transform Infrared spectroscopy (FTIR) analysis

using a Bruker Vertex 70 (Bruker, Billerica, MA, USA) equipment with a diamond ATR device in the range of 600–4000 cm^{-1}. The spectra were recorded as an average of 32 successive measurements, eliminating bands of noise, atmospheric CO_2, and atmospheric water vapor.

The morphological evaluation of the initial support membranes and the modification of pores aspect after the deposition process were revealed by High Resolution Field Emission Scanning Electron Microscopy (HR-FE-SEM). The measurements were performed on Apreo S LoVac apparatus, from Thermo Fisher Scientific, operating at acceleration voltage of 10 kV. Before analyses, a 10 nm thick layer of gold was applied on the composite membranes surface, to prevent charge accumulation during the examination process.

The chemical composition of the initial CA-GO-TiO_2 support membranes and PTFE/CA-GO-TiO_2 composite membranes was determined using X-ray Photoelectron Spectroscopy (XPS) technique. XPS analyses were done in a K-Alpha Thermo Scientific (ESCALAB™ XI+, East Grinstead, UK) spectrometer equipped with a 180° double-focusing hemispherical analyzer. The calibration of the peak positions was made with respect to the standard C1s peak (284.8 eV). Survey spectra were recorded at a pass energy of 50 eV to determine the surface elemental composition. High-resolution spectra for C1s, O1s and F1s binding energy regions were measured at pass energy of 20 eV in order to evaluate the elemental bonding states of the obtained PTFE/CA-GO-TiO_2 composite membranes. The spectra acquisition and spectra processing were performed by using the advanced Avantage data software (Thermo Avantage v5 9921, East Grinstead, UK).

IX.3 Structural and morphological characterization of nanocomposite materials based on cellulose acetate and graphene oxide and PTFE coating with TiO_2 covered

- Morphological investigations of CA-GO-TiO_2-PTFE composite membranes SEM images of the active side of CA-GO-TiO_2-PTFE composite membranes surface obtained for various GO concentration are shown in figure 95.

The SEM micrographs for the initial CA-GO-TiO_2 membranes surface reveal similar morphology for all investigated samples, with small nanometric pores present on the surface, regardless the amount of TiO_2 covered GO in the samples (Figure 95, a - c).

Still, with the increasing of graphene oxide concentration in the membranes chemical structure, a slight increasing of the apparent surface pore's diameter is observed. Moreover, the membrane's surface morphology changes from one with more compact aspect to one with more porous and aerated character.

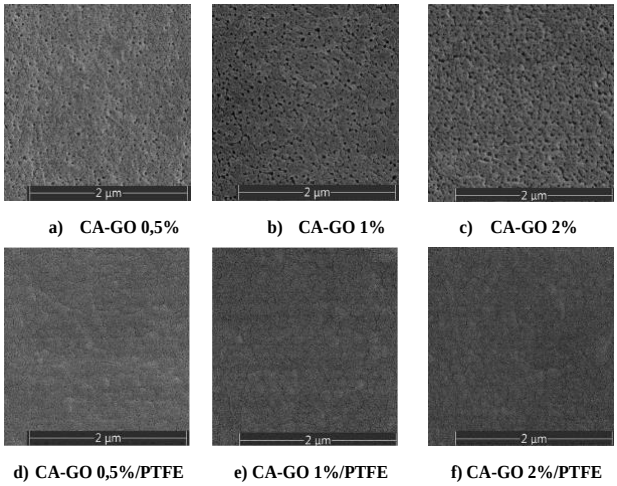

Figure 95. SEM images (magnification 50000x) of the initial CA-GO membranes (a-c) with various TiO_2 covered GO concentration on the side with small pores, and respectively of the composites membranes coated with 200 nm PTFE layer (d-f)

After the layer deposition, the surface shows a granular morphology (Figure 95, d-f) for all investigated membranes samples suggesting the uniform and controlled magnetron deposition process.

The surface apparent pores are almost completely covered, only very thin flowing channels are present on the active surface, which might ensure the wastewater transport along the pores on one hand and boosting the membranes integrity on the other hand.

The XPS survey spectra, presented in Figure 99, reveal that C and O are the main elements for the initial CA-GO support membranes, while for the PTFE-CA-GO composite membranes the surface is characterized by carbon and fluorine as major elements, with only few percents of oxygen as contaminant element, coming either from the plasma deposition process or as a consequence of surface contamination after air exposure.

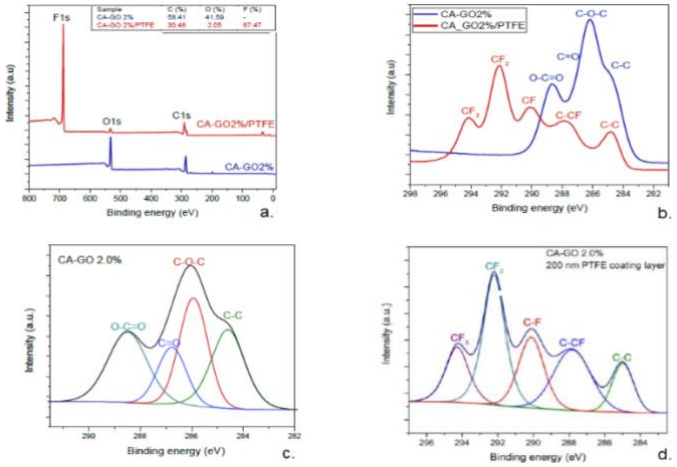

Figure 99. Comparative XPS spectra for the initial and PTFE coated CA-GO membranes: a) survey spectra and elemental concentration evidencing the modification of surface chemistry; b) C1s binding energy region and bonding identification; c) deconvolution of the initial CA GO membrane illustrating the specific peaks; d) deconvolution of the PTFE CA GO illustrating the formation of PTFE-like coating on membrane surface

The comparative high-resolution spectra for initial support membrane and PTFE coated one, presented in Figure 99b, validate the transition from a surface based on C-O bonds to one based on C-F bonds and thus confirm the obtaining of composite membranes with different surface characteristics.

The quantitative chemical bonding on the surface of the new composite membrane has been assessed by advanced processing of the high-resolution spectrum obtained for the initial and PTFE top coated CA-GO membranes.

A typical C1s high-resolution spectra recorded for the CA-GO composite membranes is displayed in Figure 99c, including its deconvolution using four components, which are counting for both CA and GO, as follows: C-C bonds at 284.8 eV, C-O-C bonds at 286.3 eV, C=O bonds at 287.7 eV and O-C=O bonds at 289 eV.

Similarly, evaluation of the chemical bonding on the surface of CA-GO/PTFE coated membranes was performed by the C1s spectrum high spectra deconvolution in five components, corresponding to: the CF_3 bond at 294 eV with a contribution of 17%, CF_2 bond at 292 eV with the most important contribution of 35%, CF bond at 290 eV with a contribution of 20%, C-CF bond at 288 eV and C-C at 285 eV with lower contribution of 16% and 12% respectively.

Additionally, FTIR technique was realized in order to evaluate in bulk composition in comparison to the data provided on the membranes surface by the XPS investigations

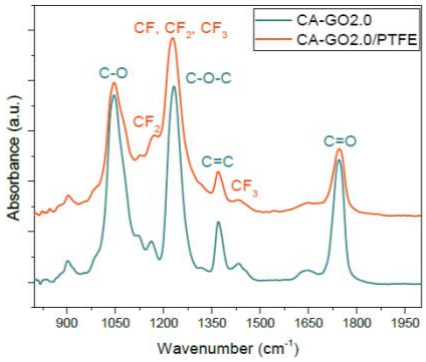

Figure 101. FTIR spectra of the CA-GO 2.0 wt.% composite membrane (blue line) and CA-GO 2.0 wt.%/PTFE TFC membrane (red line).

The typical IR spectrum for cellulose acetate polymer is dominated by four narrow and strong absorption bands, typical for the compound, evidenced in blue color, as follows: the absorption band from 1046 cm^{-1} is assigned to C-O bonds contribution, the peak situated at 1230 cm^{-1} is associated with the C-O-C bond vibration, while the contributions of C=C and C=O bonds are revealed by the absorption bands from 1371 cm^{-1} and 1745 cm^{-1}.

PTFE fingerprint, as component of the thin film composite membranes, is evidenced by the specific absorption bands, highlighted in red color, as follows, the strong vibration at 1227 cm^{-1} and the small shoulder at 1170 cm^{-1} are assigned to CF_2 symmetric and asymmetric stretching bonds. Also, CF and CF_3 bonds are superimposed to CF_2 bonds contribution, chemical structure which is typical for plasma-based PTFE material.

Additional peaks of PTFE top layer reveal the presence of CF_3 vibration at 982 cm^{-1}, while the small absorption peak at 1433 cm^{-1} is associated to CF_2 combined asymmetric stretching and rocking deformations. The FTIR investigation corroborated with those obtained by XPS technique confirms the successful preparation of the CA-GO/PTFE thin films composite membranes.

IX.4 Testing of obtained materials in the study of photocatalytic oxidation of azithromycin

The results obtained from the photocatalytic degradation tests of azithromycin using the three functionalized photocatalytic membrane materials are presented in Figures 102-104.

For the photocatalytic membrane coated with PTFE with graphene oxide in percentage of 0.5%, the results are presented in Figure 102.

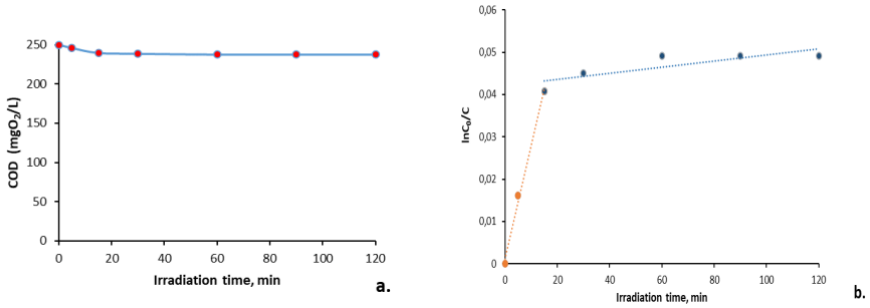

Figure 102. Kinetics of the photocatalytic degradation of the organic content of the Azitrox formulation using the CA-GO 0.5%/PTFE photocatalytic membrane: a. COD values against time; b. $\ln(C_0/C)$ against time illustrating pseudo-first-order photocatalytic reaction

For the photocatalytic membrane coated with PTFE with graphene oxide in percentage of 1%, the results are presented in Figure 103.

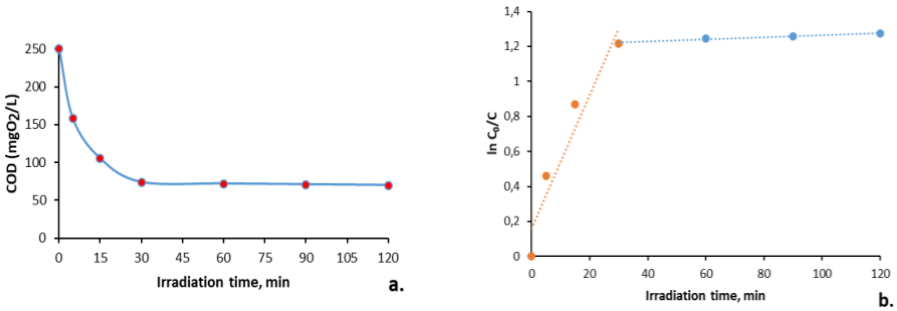

Figure 103. Kinetics of the photocatalytic degradation of the organic content of the Azitrox formulation using the CA-GO 1%/PTFE photocatalytic membrane: a. COD values against time; b. $\ln(C_0/C)$ against time illustrating pseudo-first-order photocatalytic reaction

For the photocatalytic membrane coated with PTFE with graphene oxide in percentage of 2%, the results are presented in Figure 104.

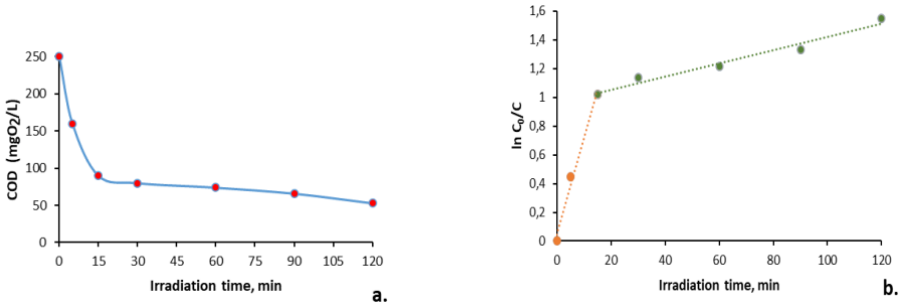

Figure 104. Kinetics of the photocatalytic degradation of the organic content of the Azitrox formulation using the CA-GO 1%/PTFE photocatalytic membrane: a. COD values against time; b. ln(C_0/C) against time illustrating pseudo-first-order photocatalytic reaction

As it can be seen, only a slight decrease in the concentration of organic material is noticed in the first 15 minutes of irradiation, after which its concentration remains almost unchanged.

The kinetic study of the photocatalytic degradation of the organic material (figure 102 b,; figure 103 b.; figure 104 b.) suggests that the degradation process is taking place in two stages with distinct rates.

In the first stage (the first 15 minutes of irradiation) the degradation of the organic content takes place quickly, while in the second stage the degradation takes place slowly. It seems that, in the first stage of photocatalytic degradation, the organic excipients from Azitrox formulations such as sugar, hydroxypropyl cellulose, starch, are playing a significant role.

These excipients can interact with the free radicals from the aqueous solution generated in the photocatalytic process by means of abstractable hydrogens from their molecule. In this way, they play the role of transfer agents of free radicals, protecting the active component (e.g. azithromycin in this case) from the pharmaceutical formulations against degradation. As soon as this protection disappears, the active component begins to degrade, and the rate is different. This could be the explanation why the organic content of the Azitrox formulation is degraded in two stages with different degradation rates.

A similar kinetics can be observed for the other two membranes, the differences being the degradation rates of the organic content for each formulation of the membrane.

The rate constants of the two degradation stages for each photocatalytic membrane are presented in Table 15.

Table 15. Pseudo-first-order rate constants for the photocatalytic degradation of the organic content corresponding to the three types of photocatalytic membranes

Pseudo-first-order rate constant (k)	Photocatalytic membranes					
	CA/GO 0.5%		CA/GO 1%		CA/GO 2%	
	Degradation stage					
	I	II	I	II	I	II
k, min^{-1}	2.7×10^{-3}	7.0×10^{-5}	5.5×10^{-2}	3.9×10^{-3}	6.7×10^{-2}	4.6×10^{-3}

As can be seen in the Table 15, that as the proportion of TiO_2 covered graphene oxide in the photocatalytic membrane increases, the rate of degradation of the organic content increases in both steps of degradation.

Thus, the rate constants of the photocatalytic degradation process of the organic content in the second stage (azithromycin) increases by almost two orders of magnitude from the PTFE coated membrane containing 0.5% GO (CA-GO 0.5%) to the PTFE coated membrane containing 1% GO (%), (CA-GO1%) and that containing 2% GO % (CA-GO-2%). More precisely, the photocatalytic reaction rate constants of the membranes with 1% GO and 2% GO are 20 and respectively 24 times higher in the first stage, and 56 and respectively 66 times in the second stage, as compared to the PTFE coated membrane with the lowest concentration (0.5%) of TiO_2 covered GO in the composition.

IX.6 Partial conclusions

A new type of photocatalytic membrane of thin film composite membranes designed from the classical phase inversion membrane based on cellulose acetate and including in bulk addition of TiO_2 covered graphene oxide, with GO ranging 0.5%, 1%, 2% and on both surfaces thin films of polytetrafluorethylene-like deposited by magnetron sputtering. This approach allows the inclusion of photocatalytical active centers in the porous support while offering chemical and thermal robustness due to the PTFE layer, without significant modification of the membrane porosity.

The results evidenced that the chemical composition, as revealed by XPS and FTIR techniques, is dominated by dominated in bulk by the carbon-oxygen bonds originating from CA and GO while the carbon-fluorine specific bonds are present on the surface upon PTFE coating. Microtomography and SEM images reveal a uniform aspect of the membranes regardless the GO amount and only slight modification of the porosity.

The kinetic studies of the photocatalytic degradation process of the organic content of the Azitrox formulation indicates a degradation in two stages with different rates, among which we associate the second stage with the degradation of the active component contained in the Azitrox formulation, namely azithromycin.

The degradation efficiency of the organic content of the Azitrox formulation increases significantly from 5% to 73% upon GO increase from 0.5% to 1%, while further increase of GO concentration to 2% conduct to its slight increase up to 80%.

The obtained results indicate that an additional increase in GO amount added to the photocatalytic membrane would not necessarily lead to a significant improvement of the properties, as agglomeration and formation of defect centers may appear in membrane bulk and diminish the thermal resistance as well as the performances in the photocatalytic reactor.

This chapter will be published as: Veronica SATULU, Andreea Madalina PANDELE, Giovanina-Iuliana LUPU, Liliana BOBIRICĂ, Anca BONCIU, Constantin BOBIRICĂ, Cristina ORBECI, Stefan Ioan VOICU, Bogdana MITU, Gheorghe DINESCU. Robust CA-GO-PTFE photocatalytic membranes for degradation of azithromycin from wastewaters. Process Safety and Environmental Protection, 2023 *F.I. 10,8*

Chapter X – General conclusions

Advanced oxidation processes can be used to remove a wide range of organic and pharmaceutical compounds from wastewater due to their high oxidation capacity. Through various combinations of oxidants and catalysts, the oxidation potential can be significantly enhanced.

Photocatalyst is one of the advanced and promising technologies for oxidation processes, having effective applications in several applications and industries, including wastewater treatment and purification. The appropriate choice of photocatalyst and the establishment of optimal operating conditions can lead to obtaining high rates of degradation of organic contaminants refractory to removal from wastewater.

In chapter IV, the influence of the operating parameters on the photocatalytic oxidation of a phenolic compound (2,4-dichlorophenol) using a TiO_2/stainless steel functionalized material was evaluated, resulting in the following conclusions:

- operating parameters (pH of the working environment, initial organic compound concentration, optimal value of the hydrogen peroxide:2,4-dichlorophenol molar ratio) have a significantly high importance, so these parameters influence the efficiency of the photocatalytic degradation process of 2,4 -dichlorophenol;
- the rate of photocatalytic degradation increases in acidic conditions (pH = 3),leading to an increase of the degradation efficiency of 2,4-dichlorophenol;

The results obtained indicated that there is an inversely proportional relationship between the rate of photocatalytic degradation and the initial concentration of organic compound, in this case 2,4-dichlorophenol.

In Chapter V, the photocatalytic activity of two functionalized photocatalytic membrane materials, namely a TiO_2/Ti-type membrane and a Co-doped TiO_2/polymer membrane, was evaluated. The following conclusions can be drawn from this study:

- The photocatalytic degradation efficiency of the two phenolic compounds (4-chlorophenol and 2,4-dichlorophenol) was higher in the case of the Co-doped TiO_2/polymer membrane than in the case of the TiO_2/Ti membrane.
- The photocatalytic degradation rate reached higher values in the case of 4-chlorophenol than in the case of 2,4-dichlorophenol, depending on the photocatalytic membrane used;
- The selection of the right photocatalyst and the establishment of optimal working conditions can lead to high values of photocatalytic degradation efficiencies of organic compounds, in this case, 4-chlorophenol and 2,4-dichlorophenol.

In Chapter VI, a series of TiO_2/fiberglass functionalized materials were synthesized, of type stratified network, type fabric and type mesh, by three different methods, with or without the existence of a subsequent treatment step. All these materials obtained were characterized from the structural and morphological point and were tested in the study of the photocatalytic oxidation of the organic content of azithromycin. The photocatalytic degradation of azithromycin was efficient, with values of up to 85% in the case of the TiO_2/fiberglass functionalized materials type mesh (3C) material prepared by immersing the support material in a TiO_2 solution. It can be stated that these functionalized materials have proven to be efficient in the study of the photocatalytic oxidation of azithromycin.

In chapter VII, were prepared two TiO_2/fiberglass functionalized materials type stratified network and TiO_2 doped with Nb/fiberglass type stratified network. These materials were characterized structurally and morphologically to confirm the uniform deposition of TiO_2 on the surface of the inert fiberglass material.

Photocatalytic degradation efficiencies were also evaluated, obtaining less satisfactory results (low values of photocatalytic degradation efficiencies).

In Chapter VIII, three functionalized materials of type Nb dopped TiO_2/fiberglass type mesh and Nb and Fe dopped TiO_2/fiberglass type mesh (two Fe concentrations) were synthesized and characterized. The preparation of these materials took place in two stages, so in the first stage the photocatalysts were prepared, and in the second stage the functionalized materials of type photocatalytic membranes were prepared, using a rubber-type silicone binder. The evaluation of the photocatalytic activity was carried out in the study

of the photocatalytic oxidation of azithromycin, obtaining average photocatalytic degradation efficiencies.

Chapter IX aimed to obtain functionalized nanocomposite materials based on cellulose acetate and graphene oxide (three different amounts) coated with a thin layer of polytetrafluoroethylene with TiO_2 embedded in the structure. These new functionalized materials were characterized structurally and morphologically, and the evaluation of the photocatalytic activity was carried out in the study of the photocatalytic oxidation of the antibiotic azithromycin. The photocatalytic degradation efficiencies of azithromycin reached values from 5% to 73%, these efficiencies being directly proportional to the amount of graphene oxide contained in each functionalized material (0.5%, 1%, 2% graphene oxide).

The experimental research carried out has highlighted the obtaining of new functionalized materials with potential application in the photocatalytic degradation of organic compounds from wastewater. Through these original contributions and experimental research included in the PhD thesis, a new perspective has been developed regarding the obtaining of functionalized materials with potential for application in the degradation and elimination of organic compounds from wastewater.

Original contributions and future development prospects

The most important element of novelty is represented by the obtaining of new functionalized materials of type TiO_2 doped with Nb/fiberglass type mesh and TiO_2 doped with Nb and Fe/fiberglass type mesh using a commercial product of type polydimethylsiloxane as a binder, as well as the structural and morphological characterization of the materials obtained, but also the testing of these materials in the study of the photo-oxidative degradation of azithromycin. In the first stage, the photocatalysts (TiO_2 doped with Nb and TiO_2 doped with Nb and Fe, with two different Fe concentrations) were synthesized, and then these photocatalysts were deposited on a glass fiber type mesh support material. The idea of using a commercial product of type polydimethylsiloxane is proprietary, resulting from attempts to create a functionalized material with high photo-oxidative activity.

Some new perspectives are listed below, namely:

- the development of new types of photocatalysts and/or photocatalytic membranes for applications in advanced wastewater treatment processes with high content of organic compounds;
- the identification of more efficient photocatalytic systems for the degradation of organic compounds that are difficult to biodegrade or non-biodegradable, used individually or combined.

List of published papers:

- Giovanina-Iuliana LUPU, Cristina ORBECI, Liliana BOBIRICĂ, Constantin BOBIRICĂ, Luoana Florentina PASCU. Key Principles of Advanced Oxidation Processes: A Systematic Analysis of Current and Future Perspectives of the Removal of Antibiotics from Wastewater. Catalysts 2023, 13(9), 1280, *F.I. 3,9*
- Giovanina-Iuliana Lupu, Liliana Bobirică, Constantin Bobirică, Cristina Orbeci. Photocatalytic oxidation of azithromycin in aqueous solution by TiO_2-coated fiberglass membrane. UPB Scientific Bulletin Series B: Chemistry and Materials Science 2023, 85(2), 35-44, *F.I. 0,5*
- Bobirică L., Bobirică C., Lupu G.I., Orbeci C., Influence of Operating Parameters on Photocatalytic Oxidation of 2,4-Dichlorofenol in Aqueous Solution by TiO_2/Stainless Steel Photocatalytic Membrane. Applied Sciences 2021, 11(24), 11664, *F.I. 2,7*

Participation of international scientific conferences:

- C. Orbeci, G.I. Lupu, C. Bobirică, L. Bobirică, Ivermectin removal from wastewater by photocatalytic degradation, 4th International Conference on Environmental Design ICED 2023, Atena, Grecia, 20-22 October 2023
- Giovanina-Iuliana Lupu, Cristina Orbeci, Liliana Bobirică, Constantin Bobirică, Azithromycin removal from wastewater by photocatalic degradation, 26th International Symposium “Environment and Industry”, Bucharest, România, 27-29 September 2023
- V. Satulu, A.M. Pandele, A. Bonciu, S.I. Voicu , G.I. Lupu, L. Bobirica, C. Bobirica, C. Orbeci, B. Mitu, G. Dinescu. Robust CA-GO-PTFE membranes for azithromycin photo-

degradation in wastewaters, E-MRS 2023 - Spring Meeting - SYMPOSIUM C, Advanced materials for environmental challenges, Strasbourg, Franța, 29 May-2 june 2023

- Giovanina-Iuliana Lupu, Liliana Bobirică, Constantin Bobirică, Cristina Orbeci, Ecaterina Matei, Maria Râpă, Photocatalytic oxidation of azithromycin in aqueous solution by TiO_2-coated fiberglass membrane, Romanian International Conference on Chemistry and Chemical Engineering RICCCE 22, Sinaia, România, 7-9 September 2022
- Cristina Orbeci, Liliana Bobirică, Constantin Bobirică, Giovanina-Iuliana Lupu, Evaluation of TiO_2-Photocatalytic Membrane to Removal of 2,4-DCP from Wastewater, Romanian International Conference on Chemistry and Chemical Engineering RICCCE 22, Sinaia, România, 7-9 September 2022
- Giovanina-Iuliana Lupu, Liliana Bobirică, Constantin Bobirică, Cristina Orbeci, Removal of chlorophenols from aqueous solutions by photocatalytic oxidation, 5th International Conference of the Doctoral School, Iași, România, 18-20 May 2022
- Giovanina-Iuliana Lupu Workshop: Summer School Nonlinear Life 4th edition – online edition, Bergamo, Italy – Curs ,,Advances in materials for medicine'' 26-29 July 2021

References

1. V. Kumar, M.P. Shah, 1 - Advanced oxidation processes for complex wastewater treatment in Advanced Oxidation Processes for Effluent Treatment Plants, Elsevier, 2021, pp. 1-31, https://doi.org/10.1016/B978-0-12-821011-6.00001-3
2. S.C. Ameta, R. Ameta, Advanced Oxidation Processes for Wastewater Treatment 1st Edition, publishing by Academic Press, 2018
3. T.S. Rajaraman, V. Gandhi, S.P. Parikh, Advanced Oxidation Processes for Wastewater Remediation: Fundamental Concepts to Recent Advances, Materials Research Foundations, vol. 91, 2021, pp. 37-86,
4.M. Kurian, Advanced oxidation processes and nanomaterials - a review, Clean. Eng. Technol., vol. 2, 2021, 100090, https://doi.org/10.1016/j.clet.2021.100090
5. L.L. Jiao, P.C. Zhao, Z.Q. Liu, Q.S. Wu, D.Q. Yan, Y.L. Li, Y.N. Chen, J.S. Li, Preparation of Magnesium Hydroxide Flame Retardant from Hydromagnesite and Enhance the Flame Retardant Performance of EVA, Polymers, vol. 14, 2022, 1567, https://doi.org/10.3390/polym14081567
6. A.S. Khaliullina, L.A. Dunyushkina, Preparation of a film electrolyte based on calcium zirconate on a porous electrode by a chemical liquid-phase method, Russ. J. Appl. Chem., vol. 90, 2017, pp. 1674–1679, https://doi.org/10.1134/S1070427217100172
7. Q. Meng, J. Wang, Synthesis of Fe-doped ZnO by parallel flow precipitation method and its photocatalytic denitrification performance, CIESC J., vol. 68, no. 1, pp. 437–443, doi: 10.11949/j.issn.0438-1157.20161231
8. M.S. Lassoued, A. Lassoued, S. Ammar, A. Gadri, A.B. Salah, S. García-Granda, Synthesis and characterization of co-doped nano-TiO_2 through co-precipitation method for photocatalytic activity, J. Mater. Sci. Mater. Electron., vol. 29, 2018, pp. 8914–8922, https://doi.org/10.1007/s10854-018-8910-x
9. K. Wenderich, G. Mul, Methods, mechanism, and applications of photodeposition in photocatalysis: A review, Chem. Rev., vol.116, no. 23, 2016, pp.14587–14619, https://doi.org/10.1021/acs.chemrev.6b00327
10. Z. Frontistis, New Trends in Environmental Catalytic Technologies for Water Remediation, Water, vol. 13, no.4, 2021, 571, https://doi.org/10.3390/w13040571
11. C. Orbeci, C. Bobirică, L. Bobirică, Photocatalytic Degradation of Chlorophenols and Antibiotics from Wastewater, in Inamuddin, Ahamed, M.I., Lichtfouse, E. (eds) of Water Pollution and Remediation: Photocatalysis. Environmental Chemistry for a Sustainable World, vol 57. Springer, pp. 411-429, https://doi.org/10.1007/978-3-030-54723-3_13
12. M. Zhuang, D. Ren, H. Guo, Z. Wang, S. Zhang, X. Zhang, X. Gong, Degradation of 2,4-dichlorophenol contaminated soil by ultrasound-enhanced laccase, Environmental Technology, vol. 42, no. 9, 2021, pp.1428-1437, https://doi.org/10.1080/09593330.2019.1669723
13. R. K. Langbehn, C. Michels, H. M. Soares, Antibiotics in wastewater: From its occurrence to the biological removal by environmentally conscious technologies, Environmental Pollution, vol.275, 2021, 116603, https://doi.org/10.1016/j.envpol.2021.116603

14. D.N. Vangapandu, M. Paul, P. Mishra, R. Sarathi, A. Paramane, M. T. Nazir, Performance Evaluation of Thermally aged RTV Silicone Rubber/TiO_2 Nanocomposites in Mineral Oil for Transformer Bushings, IEEE Transactions on Dielectrics and Electrical Insulation, vol. 30, no.4, 2023, pp. 1493-1501, doi: 10.1109/TDEI.2023.3277803
15. S. Ruzgar, S. A. Pehlivanoglu, The effect of Fe dopant on structural, optical properties of TiO_2 thin films and electrical performance of TiO_2 based photodiode, Superlattices and Microstructures, vol.145, 2020, 106636, https://doi.org/10.1016/j.spmi.2020.106636
16. 114. J. Chen, Y. Xiong, M. Duan, X. Li, J. Li, S. Fang, S. Qin, R. Zhang, Insight into th Synergistic Effect of Adsorption Photocatalysis for the Removal of Organic Dye Pollutants by Cr-Doped ZnO, Langmuir: ACS journal of surfaces and colloids, vol. 36, no. 2, 2019, 520–533. https://doi.org/10.1021/acs.langmuir.9b02879Wang, X. Zhang, F. Wang, X. Lan, Chemical characterization and research on the silicone rubber material used for outdoor current transformer insulation, Phosphorus, Sulfur, and Silicon and the Related Elements, vol. 192, no.1,2017, pp. 109-112, https://doi.org/10.1080/10426507.2016.1231189
17. A. Zada, M. Khan, M.A. Khan, Q. Khan, A.H. Yangjeh, A. Dang, M. Maqbool, Review on the hazardous applications and photodegradation mechanisms of chlorophenols over different photocatalysts, Environmental Research, vol. 195, 2021, 110742, https://doi.org/10.1016/j.envres.2021.110742
18. M. Manna, S. Sen, Advanced oxidation process: a sustainable technology for treating refractory organic compounds present in industrial wastewater, Environ. Sci. Pollut. Res., vol. 30, 2023, pp. 25477–25505. https://doi.org/10.1007/s11356-022-19435-0
19. M. Cai, H. He, X. Zhang, X. Yan, J. Li, F. Chen, D. Yuan, X. Ning, Efficient synthesis of PVDF/PI side-by-side bicomponent nanofiber membrane with enhanced mechanical strength and good thermal stability, Nanomaterials, vol.9, no.1, 2019, 39, https://doi.org/10.3390/nano9010039
19. C. Maheu, L. Cardenas, E. Puzenat, P. Afanasiev, C. Geantet, UPS and UV spectroscopies combined to position the energy levels of TiO_2 anatase and rutile nanopowders, Phys. Chem. Chem. Phys., vol. 20, no. 40, pp. 25629–25637, https://doi.org/10.1039/C8CP04614J
20. A. Muñoz-Calderón, H. Zúñiga-Benítez, S. H. Valencia, A. R. Clemente, S. A. Upegui, G. A. Peñuela, Use of low frequency ultrasound for water treatment: Data on azithromycin removal, Data in Brief, vol. 31, 2020, 105947, https://doi.org/10.1016/j.dib.2020.105947
21. N.C. Zheng, T. Ouyang, Y. Chen, Z. Wang, D.Y. Chen, Z.Q. Liu, Ultrathin CdS shell-sensitized hollow s-doped CeO_2 spheres for efficient visible-light photocatalysis, Catal. Sci. Technol., vol. 9, 2019, pp.1357–1364, https://doi.org/10.1039/C8CY02206B
22. L.L. Jiao, P.C. Zhao, Z.Q. Liu, Q.S. Wu, D.Q. Yan, Y.L. Li, Y.N. Chen, J.S. Li, Preparation of Magnesium Hydroxide Flame Retardant from Hydromagnesite and Enhance the Flame Retardant Performance of EVA, Polymers, vol. 14, 2022, 1567, https://doi.org/10.3390/polym14081567
23. S. I. Polianciuc, A. E. Gurzău, B. Kiss, M. G. Ştefan, F. Loghin, Antibiotics in the environment: causes and consequences, Medicine and pharmacy reports, vol. 93, no.3, 2020, pp.231–240, https://doi.org/10.15386/mpr-1742
24. J. Chen, Y. Xiong, M. Duan, X. Li, J. Li, S. Fang, S. Qin, R. Zhang, Insight into th Synergistic Effect of Adsorption Photocatalysis for the Removal of Organic Dye Pollutants by Cr-Doped ZnO, Langmuir: ACS journal of surfaces and colloids, vol. 36, no. 2, 2019, 520–533. https://doi.org/10.1021/acs.langmuir.9b02879
25. J. Fu, Y. Zhao, Q. Yao, O. Addo-Bankas, B. Ji, Y. Yuan, T. Wei, A. Esteve-Núñez, A review on antibiotics removal: Leveraging the combination of grey and green techniques, Science of The Total Environment, vol. 838, no. 3, 2022, 156427, https://doi.org/10.1016/j.scitotenv.2022.156427